UNIVERSITY OF OKLAHOMA

GRADUATE COLLEGE

COMPARATIVE ANALYSIS OF QUANTUM COMPRESSIVE IMAGING IN LOW PHOTON REGIME BY CONSIDERING PHOTON STATISTICS

A THESIS

SUBMITTED TO THE GRADUATE FACULTY

in partial fulfillment of the requirements for the

Degree of

MASTER OF SCIENCE

By

VAMSI KRISHNA MANTHAPURAM
Norman, Oklahoma
2016

COMPARATIVE ANALYSIS OF QUANTUM COMPRESSIVE IMAGING IN LOW PHOTON REGIME BY CONSIDERING PHOTON STATISTICS

A THESIS APPROVED FOR THE
SCHOOL OF ELECTRICAL AND COMPUTER ENGINEERING

BY

_____
Dr. Kam Wai Clifford Chan, Chair

_____
Dr. Pramode Verma

_____
Dr. Robert Huck

Acknowledgements

Firstly, I would like to express my sincere gratitude to my advisor and committee chair Dr. Kam Wai Clifford Chan, who has inspired and introduced me to the exciting world of Quantum Compressive Imaging. He has always encouraged me by sharing his opinions and making a right move in the research work. His immense support and guidance have given me strength to complete my Master's thesis. It was a pleasure working with him.

Besides my committee chair, I would like to thank the other two committee members Dr. Pramode Verma, and Dr. Robert Huck, who have given me an opportunity to work in the Interoperability Lab and who have encouraged and guided me throughout my graduate degree program.

I would like to thank all my colleagues, Kyrus M. Kuplicki, Lu Zhang, and Bhagyashri Arun Darunkar, who have guided and supported me regarding the improvement of my thesis. In addition, they have given me suggestions concerning the writing of this thesis.

Finally, I would like to thank my parents, Srinath Manthapuram, and Rekha Manthapuram, for all the moral support and encouragement they have given me over the years.

Table of Contents

List of Tables

List of Figures

Abstract

Compressive Imaging has been an extensively researched area in optical imaging, object tracking, satellite applications, etc. There are many signal recovery methods and comparative analyses of different algorithms in the presence of Gaussian noise. However, certain applications such as optical imaging at low photon intensity have counts of discrete events, which cannot be modelled using a Gaussian noise model. Instead, a noise model that incorporates photon statistics is needed. Researchers have worked on the Poisson noise model and a different compressive sensing reconstruction was found.

In this thesis, we considered a more general scenario of Compressive Imaging using non-classical photon states as light sources. We assumed that the Compressive Imaging system that consists of digital micro mirror device (DMD), lenses, and detectors are perfect so that all noises comes from photons. Fock states and squeezed light that possess non-Poissonian statistics plays an important role in Quantum Imaging. The image reconstruction was performed using several common compressive sensing signal reconstruction algorithms assuming Gaussian noise. This thesis showed the behavior of the root mean square error (RMSE) with respect to the signal-to-noise ratio (SNR) for different photon statistics. In particular, the study showed that all the noises perform similarly for the different algorithms.

Based on the performance results for the different light sources, this research can be helpful in designing a generalized Compressive Sensing model incorporating the photon statistics that are applicable in the field of Quantum Optics.

1. Introduction

Today's world is data driven. In many emerging applications such as medical imaging, video, data analysis, spectroscopy etc., the amount of data generated is too high. The resulting Nyquist rate is so high that we end up with far many samples. This will pose a tremendous challenge, as it is extremely difficult to build such devices that are capable of acquiring samples at the necessary rate. We can overcome this computational challenge especially in dealing with high-dimensional data by "Compression" techniques. The most popular technique used for signal compression is transform coding (which finds a basis that gives the sparser representation of signal). Some of the common compression techniques such as JPEG, JPEG2000, and MPEG etc. are based on sparse transform coding. Using the same concept of sparse transform coding, a new framework is emerged for signal/image acquisition i.e., Compressive Sensing (CS). The idea of CS originates from approximation theory and was brought into forefront by E. Candès, J. Romberg, T.Tao and D. Donoho [1, 2].

In this thesis, we deal with imaging, as it has been an extensively researched area, which has contributed to technical advancement in the field of medical imaging, object tracking and satellite applications, etc. Image recognition, restoration, and reconstruction from projections are a few areas that are looked at in a different perspective after the introduction of compressive imaging. It selects the most important data from the data set i.e., for an image with $128 \times 128 = 16384$ pixels, only the most important data is considered for the image reconstruction process, thereby omitting the zero values (which are obtained by sparse representation of an image in some basis).

This is similar to data modelling/analysis where we extract the most important data from a huge data set.

Compressive Imaging has wide range of applications. It is particularly useful in low-photon imaging where the number of samplings is limited. Applications in such domain include (1) Compressive Ghost Imaging with entangled photons [3] – The conventional Ghost Imaging consists of an object arm and reference arm where the intensities of light beam are collected by the bucket detector of object arm and are cross-correlated with the intensities measured by the CCD camera at the reference arm that has spatial resolution field. In Compressive Ghost Imaging, the Spatial Light Modulator (SLM) is used and is controlled by a computer. The compressive ghost imaging gives better results than the conventional approach [4], (2) object tracking – It is the most researched topic in the field of computer vision. The purpose of object tracking is to track the objects with specific representation or estimate information from the object. Many novel CS based object-tracking algorithms were developed [5], medical imaging – a good example of it is MRI, as it requires significant amount of time to produce best quality image [6]. CS has proven to provide better image quality thereby significantly reducing the time to acquire samples, and single pixel camera (see Chapter 4.1), etc. Many robust algorithms were developed in CS, which are designed by considering the Gaussian noise model. However, many applications consists of count of discrete events, which cannot be modelled using Gaussian noise model. Instead, Poisson noise model is required [7].

There are many comparative analyses of several algorithms in addition of Gaussian noise [8-12]. With the advent of the several algorithms in Compressive

Sensing field, the main motivation of the thesis to know the robustness of the algorithms (explained in Chapter 3) in the presence of photon noise by considering photon statistics [13]. In addition, comparative analysis and the detection of an object in low photon regime (low SNR) are described. The observations analyzed from the plots of CS algorithms for various noise sources would help in determining the best noise model for image reconstruction. As researchers have worked on Poisson noise models for Compressive Imaging framework, the observations made from this thesis would help in designing a generalized Compressive Imaging model that incorporates photon statistics.

1.1 Contributions

The valuable contributions of this thesis are listed as follows:

1) Comparative analysis of the algorithms without addition of noise for two different objects (grayscale object and the binary object – The University of Oklahoma OU logo).
2) Comparative analysis of the algorithms in presence of various noise models (Gaussian, Fock states, Poisson, thermal light and squeezed light) in the low photon regime for detecting an object by studying its photon statistics.
3) Study of the general behavior of the image reconstruction (measured by the root mean squared error (RMSE)) with respect to the photon statistics (measured by the signal-to-noise ratio (SNR)) for the different light sources.

1.2 Organization of thesis

This thesis is arranged into five chapters

In Chapter 2, a general idea of the compressive sensing framework is given. The mathematical formulations used in the compressive imaging framework are introduced. Next, important properties such as the sparsity, incoherence and Restricted Isometric Property were described. Finally, the norm minimization methods were explained using the geometric representation, which are convex programming methods.

In Chapter 3, current existing optimization algorithms which are alternatives of $l1$ minimization algorithms, are described. The algorithms include Greedy algorithms, thresholding algorithms, gradient pursuit and Bayesian algorithms.

In Chapter 4, a brief description of the properties of the different light sources (Fock, Gaussian, Poisson, and squeezed light) along with SNR formulations that are used in our simulations are explained.

In Chapter 5, the binary object (OU logo image), and gray scale object are considered for the comparative analysis of different algorithms with and without addition of noise. All the graphs are log log plotted for the two images for different algorithms by considering SNR on x-axis and Root Mean Square Error (RMSE) on y-axis. Also, the reconstructed image results are shown.

In Chapter 6, the conclusion of all the results in noisy case and future works are given.

2. Theory of Compressive Sensing

Compressive Sensing (CS) also known as Sparse Signal Sampling is a new framework to reconstruct signals accurately and efficiently with less number of samples i.e., less than the Nyquist rate. According to the Shannon Nyquist sampling theorem, a signal can be reconstructed at a rate of twice the highest frequency of the signal.

Generally, compressive sensing works with sparse signals. In many applications the signal of interest is sparse i.e., the signal has a sparse representation in some pre-determined basis where most of the coefficients are zero. Traditional measurement techniques oversample the signal heavily. Compressive sensing technique avoids excessive oversampling by linear sampling operators.

One of the breakthroughs in compressive sensing is by E. Candès, J. Romberg, T.Tao and D. Donoho in 2006 [2, 14], who showed Linear programming methods can be used to reconstruct the signal data efficiently with high accuracy. Since then many faster methods were proposed as alternatives to these linear programming algorithms.

This chapter will give a general idea on the mathematical formulation, properties and norm minimization methodologies of Compressive Sensing.

2.1 Compressive Imaging

Many natural images are sparse in some basis and are reconstructed efficiently using Compressive Sensing framework. The CS framework has two major steps The first is Signal Acquisition – it is the process of acquiring compressed measurements and it is known as sensing. The second is Reconstruction – that is recovering of the original sparse signal from compressed measurements and is known as reconstruction.

A 1-D signal x can be represented as a $N \times 1$ column vector in R^N. Since this thesis deals with 2-D images in the CS framework, the author uses the name Compressive Imaging. The 2-D images are treated as higher dimensional data by vectoring it into a one-dimensional vector R^N and are represented in terms of basis of $N \times 1$ vector. A basis is a $N \times N$ matrix (discrete cosine transform, wavelet, canonical etc.) which makes an image sparse. In this thesis, I have considered wavelet basis for sparse representation of an image. An image x can be expressed as

$$x = \psi s, \tag{2.1}$$

s is a sparse representation of an image $N \times 1$ and ψ is $N \times N$ wavelet basis.

The main compressive imaging framework is expressed by the following equation.

$$y = \varphi x = \varphi \psi s, \tag{2.2}$$

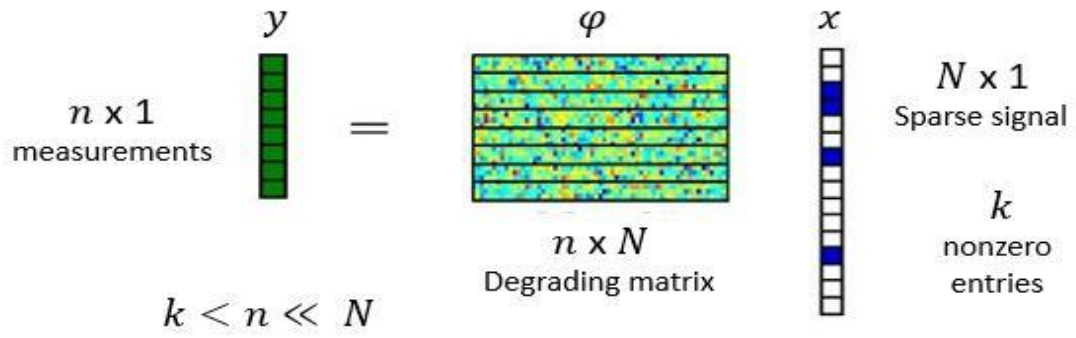

Figure 1. General representation of y

where φ is a degrading matrix of size $n \times N$ in $R^{n \times N}$ which under-samples the sparse image less than the Nyquist rate. The resultant y will be a low dimensional matrix of size $n \times 1$ in R^n. Since there are more unknowns than measurements, the system is classified as an undetermined system. It is clear that we cannot obtain an accurate input image using the conventional inverse transform. Instead, we can obtain an input image

using compressive imaging algorithms from fewer measurements. The optimization algorithms are explained in Chapter 3.

There are two fundamental properties underlying compressive imaging: Sparsity and Incoherence.

2.1.1 Sparsity

Sparsity is a general modeling tool for efficient signal processing (efficient data compression, accurate statistical estimation and classification) [1]. An image is compressible if it is sparse in some basis such as the discrete cosine transform (DCT), wavelet, curvelet etc. Mathematically, a vector $x \in R^n$ is expanded in basis $\psi = [\psi 1\ \psi 2\ ...\ \psi_N]$ and s is expressed as:

$$s = \psi^T x, \tag{2.3}$$

in which s is the weighing coefficients of an image.

If we consider DCT, it converts the pixels in an image into sets of spatial frequencies. The DCT works by separating images into parts of different frequencies. During the step of quantization, where the parts of the compression actually occur, the less important frequencies are discarded. The important frequencies that remain are used to retrieve the image in the decomposition process. The main disadvantage of DCT is that it introduces block artifacts and the computational time involved in the reconstruction process is high. In the case of the wavelet basis, it decomposes an image into two parts – a set of low frequencies and a set of high frequencies. If we are interested in the low frequency part, we can discard the high frequencies and the same way the other. Compared to DCT, the wavelet basis provide better results in terms of properties like the root-mean-squared (RMS) error, image intensity and execution time.

In addition, the wavelet transform overcomes the block artifacts that are introduced in the reconstructed image by DCT.

When an image has a sparse expansion in the wavelet basis, most of its coefficients are small and relatively few larger coefficients capture most of the information. Therefore, one can discard the smaller coefficients without any perceptual loss. A vector is sparse if it has fewer numbers of non-zeros than the number of zeros. By putting all together, we can say that the image is k-sparse when it satisfies this condition: $k < n \ll N$.

2.1.2 Incoherence

We have a pair of orthonormal bases (φ, ψ). The symbol φ is for sensing the object x and ψ is the representation of the object x. The coherence between the pair of the bases (φ, ψ) is expressed by the following equation

$$\mu(\varphi, \psi) = \sqrt{N}. \max_{1 \le i, j \le N} |\langle \varphi_i, \psi_j \rangle|, \tag{2.4}$$

Compressive Imaging is mostly concerned with low incoherence pairs. If the bases φ and ψ contain correlated elements, it has high coherence. Otherwise, they are less coherent. From linear algebra, the coherence between the bases are bounded with $\mu(\varphi, \psi) \in [1, \sqrt{N}]$. If we consider noiselets for φ and wavelets for ψ then the coherence between them is $\sqrt{2}$. Similarly if we consider noiselets and daubechies D4 and D8 wavelets, then the coherence between them is 2.2 and 2.9 respectively [1].

2.2 Restricted Isometric Property (RIP)

In addition to sparsity and incoherence, there is one more property that has to be satisfied i.e., the Restricted Isometric Property. Candès and Tao introduced the isometry conditions on the matrices φ and established its important role in compressive sensing.

In some of the papers, the Restricted Isometric Property (RIP) is the same as the Uniform Uncertainty Principle (UUP). The RIP matrices squash the sparse vectors from higher dimensional space into a lower dimensional space while being able to reconstruct the vectors [15].

RIP matrix has n rows and N columns ($n \ll N$). For a given matrix φ and T which is a set of column indices, φ_T where $T \subset \{1, \ldots, N\}$ be $N \times |T|$ submatrix obtained by extracting the columns of φ corresponding to indices in T. Similarly, the vector x in R^N is denoted by the vector x_T obtained by retaining the entries in x corresponding to the column indices in T. A matrix φ is said to be k-RIP (k number of non-zeros) if there exists a $\delta_k \in (0,1)$ and satisfy the following inequality

$$(1 - \delta_k)||x_T||_2^2 \leq \left||\varphi_T x_T|\right|_2^2 \leq (1 + \delta_k)||x_T||_2^2, \tag{2.5}$$

Good matrices for compressive sensing should satisfy the above inequality for the largest possible value of k.

There are several constructions for the RIP matrices such as the random normalized Gaussian matrices, the random normalized Fourier matrices, the Rademacher matrices etc. It is important to know which matrices obey the RIP with good isometric constants. If φ is a Gaussian random matrix, then stable recovery occurs for all φ's provided that the number of non-zeros of x are of the same order as the number of observations with $k \leq C.\frac{n}{\log(\frac{N}{n})}$. If φ is a random Fourier transform matrix with few Fourier samples of x, then stable recovery occurs for n coefficients provided that the number of non-zeros is of order $K \leq C.\frac{n}{(logN)^6}$.

Mostly, random processes are used to produce Restricted Isometric Property matrices. Deterministic matrices are also used, but only limited to smaller sparsity levels. For higher sparsity levels, random process would be a better choice and so is Gaussian random matrices. Along with this RIP, incoherence is also an important property which I mentioned earlier section 2.1.2

It is important to note that verifying the RIP may be a difficult task and also there is no fast algorithm that tests whether a given matrix satisfies the RIP or not [16].

2.3 Norm minimization

Generally, a norm is used to measure the strength of a signal or the size of an error. When dealing with vectors in R^N, we will make frequent use of l_p norms for $p \in [1, \infty)$. The geometrical representation of some examples of norm minimizations appears in the following figure.

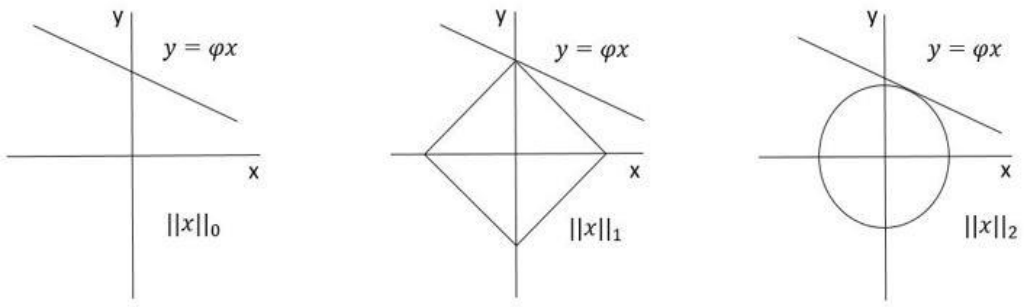

(a) **(b)** **(c)**

Figure 2. (a), (b) and (c) are l0 norm, l1 norm and l2 norm minimization respectively.

From (2.2) we can say, it is a linear problem where φ is a degrading matrix and x is a vector. It is an under-determined system, which means there are more variables

than equations. One can solve this by norm minimization methods, which the author explains in the sub sections.

2.3.1 l_0 norm minimization

In general l_0 minimization is not considered as a norm. The following is the l_0 minimization problem.

$$\min_x ||x||_0 \ s.t \ \ y = \varphi x, \tag{2.6}$$

in which $||x||_0$ represents the number of non-zero entries in x which is also called the sparsity of vector. If the vector x is k- sparse, we need to search $\binom{N}{k}$ possibilities which means the algorithm grows as $\binom{N}{k}$ with increase in k. This is a combinational problem; hence, the computational complexity with l_0 norm regularization is NP Hard.

2.3.2 l_1 norm minimization

Since l_0 norm is non-convex and it is known that non-convex problems are computationally difficult to solve, an alternative is to use convex l_1 optimization problem. l_1 norm minimization yields the sparsest recovery solution for large number problems if the solution of x is sparse enough. The following is the l_1 minimization problem.

$$\min_x ||x||_1 \ s.t \ \ y = \varphi x, \tag{2.7}$$

From Figure 2, we see that the line of solutions touches the l_1 ball. It is highly probable that the data set solutions intersect the sharp contour of the l_1 ball which results in sparser solutions. When we get exact sparse recovery solutions, the mean square error lessens. In a simpler way, we can say that l_1 norm minimization tends to concentrate the signal energy on to a fewer non-zero coefficients. l_1 norm minimization is advantageous

because it is a convex optimization problem. The complexity associated with this linear program is about $O(N^3)$.

2.3.3 l_2 norm minimization

l_2 norm minimization is preferable if the signal data is not sparse enough. The following is the l_2 minimization problem.

$$\min_x ||x||_2 \ s.t \ y = \varphi x, \tag{2.8}$$

From Figure 2, we see that the line of solution (data set) touches the l_2 ball. It is very less probable that the data set solutions intersect the axis, which results in extra non-zero elements. In a simpler way, we can say that signal energy is spread around; therefore, it is difficult to satisfy the condition of sparsity for l_2 norm.

Another alternative to the sparsest solution is by using Greedy algorithms such as Matching Pursuit (MP), Orthogonal Matching Pursuit (OMP), Iterative Hard Thresholding (IHT), Compressive Sampling Matching Pursuit (CoSaMP) etc. Likewise, many robust algorithms were developed in terms of complexity, implementation cost, speed etc. Each algorithm has its own advantages and disadvantages. The algorithms which I used in my thesis will be explained in Chapter 3.

3. CS Reconstruction Algorithms

Convex problem techniques are methods for computing a sparse representation of the signal/image. Several reconstruction algorithms were proposed in the CS framework; alternative to the convex optimization problem that are faster and give superior performance characteristics.

This chapter explains several representative algorithms that will appear extensively in the rest of the thesis. These algorithms include greedy algorithms, shrinkage/thresholding algorithms, gradient projection algorithms and wavelet based compressive sensing algorithms.

3.1 Greedy Algorithms

Greedy algorithms operate by iteratively choosing the columns of a matrix and after each iteration, the column which reduces the approximation error the most is chosen [17]. Examples of the greedy algorithms are Matching Pursuit (MP) and Orthogonal Matching Pursuit (OMP), which the author explains below.

3.1.1 Matching Pursuit algorithm

The Matching Pursuit (MP) algorithm was first introduced by Mallat and Zhang (1992) [9] which is the simplest and purest greedy algorithm in the approximation theory. The fundamental vector used in the Matching Pursuit algorithm is a residual vector, which represents the remaining part of y after updating the solution vector. MP starts from a zero solution and initializes the residual with the measurement vector y. At the end of each iteration, the column that is highly correlated with the residual is chosen from the dictionary. Each iteration consists of two steps: (i) atom selection – finds the

atom (column) that has the highest correlation with the current residual error and (ii) residual update – updates the residual error by subtracting the correlated part from it.

MP algorithm repeatedly selects the same columns from φ in order to further refine the approximation. The residual update would converge linearly to zero whenever the columns of φ span R^n. Therefore, the MP will stop in a finite number of iterations if the norm of the residual update is used to define the stopping criterion for the algorithm [12]. The main drawback of the Matching Pursuit algorithm is its slow convergence and poor sparsity result due to its sub-optimality. The pseudo-code of the MP algorithm is shown below.

Matching Pursuit (MP) algorithm

Input: $y \in R^n, \varphi \in R^{nxN}$ and termination threshold of residual norm

Output: Sparse vector $x^{[i]}, r^{[i]}$

Initialization: $x^{[0]} = 0, r^{[0]} = y, i = 1$

Compute the correlation vector: $g^{[i]} = \varphi^T r^{[i-1]}$

Find the column of matrix φ that is correlated with residual vector:

$$j^{[i]} = argmax_j \frac{|g_j^{[i]}|}{||\varphi_j||_2}$$

Update the ith solution coefficient: $x_{j^{[i]}}{}^{[i]} = x^{[i-1]} + g_{j^{[i]}}^{[i]} / ||\varphi_{j^{[i]}}||_2^2$

Compute new residual vector: $r^{[i]} = r^{[i-1]} - \varphi_{j^{[i]}} g_{j^{[i]}}^{[i]} / ||\varphi_{j^{[i]}}||_2^2$

3.1.2 Orthogonal Matching Pursuit algorithm

A modified version of the MP algorithm is proposed to limit the number of the required iterations by adding an orthogonalization step, known as the Orthogonal

Matching Pursuit (OMP) algorithm. Many steps were inherited in OMP from the MP algorithm. OMP starts from the zero solution same as in MP and initializes the residual with the measurement vector y. At the end of each iteration, OMP gives the optimal approximation with respect to the subset of selected dictionary elements by making the residue orthogonal to the chosen dictionary elements. Like MP, OMP selects the atom in the same manner. The main difference between MP and OMP is that it never reselects an atom in its subsequent iterations [12].

The main advantage of OMP over MP is that it converges in a fewer number of iterations. Though computational cost and the storage cost involved with OMP is larger than MP, it enjoys superior performance than MP, particularly in the CS framework. For a large scale of data, the computational cost and the storage cost of a single iteration of OMP is quite high [17]. The pseudo-code of the OMP algorithm is shown below.

Orthogonal Matching Pursuit (OMP) algorithm

Input: $y \in R^n, \varphi \in R^{nxN}$ and termination threshold of residual norm

Output: Sparse vector $x^{[i]}, r^{[i]}$

Initialization: $x^{[0]} = 0, r^{[0]} = y, i = 1, I^{[0]} = \emptyset$

Compute the correlation vector: $g^{[i]} = \varphi^T r^{[i-1]}$

Find the column of matrix φ that is correlated with residual vector:

$$j^{[i]} = argmax_j \frac{|g_j^{[i]}|}{||\varphi_j||_2}$$

$$I^{[i]} = I^{[i-1]} \cup j^{[i]}$$

Solve least squares problem: $x_{T^{[i]}}^{[i]} = \varphi_{T^{[i]}}^{\dagger} y$

Compute new residual vector: $r^{[i]} = y - \varphi x^{[i]}$

The table below shows the computational and storage costs of the greedy algorithms.

Algorithm	Computational Cost	Storage Cost
Matching Pursuit (MP)	$n + \varphi + N$	$\varphi + n + 2p + N$
Orthogonal Matching Pursuit (OMP)	$2np + n + \varphi + N$	$2(n+1)p + 0.5p(p+1) + \varphi + N$

Table 1. Computational cost and storage costs of greedy algorithms

where p refers to the size of the support set in the current iteration [17] and φ is the computational cost of applying or storing the transform $\varphi \; or \; \varphi^T$.

Both MP and OMP update their coefficients differently by minimizing the squared error criterion $||y - \varphi x^{[i]}||_2^2$. In MP, the minimization involves only the coefficient of the most recently selected element whereas in OMP, the minimization involves the coefficients for all selected elements at iteration i.

3.2 Shrinkage/Thresholding Algorithms

Another type of algorithm for image restoration and linear inverse problems that handle convex unconstrained optimization problems is known as Iterative shrinkage/thresholding (IST) algorithms. This type of algorithms uses a combination of linear observation parameter and nonquadratic regularizer such as wavelet-based regularization etc. The IST algorithm can be formulated to define a solution x as a minimizer of convex objective function f given below:

$$f(x) = \frac{1}{2}||y - \varphi x||^2 + \lambda||x||_1, \tag{3.1}$$

in which λ is the regularization parameter that controls the relative weight between two terms.

The IST algorithm has the form

$$x_{i+1} = (1-\beta)x_i + \beta\psi_\lambda(x_i + \varphi^T(y - \varphi x_i))$$

When $\beta = 1$ in the above equation, it is the original version of the IST algorithm

When $\beta \neq 1$ in the above equation, it can be seen as a relaxed version of IST algorithm

The computational effort involved in solving the equation is the matrix-vector multiplications involving $\varphi \; and \; \varphi^T$. In wavelet-based methods, ψ_λ is a shrinking operator. Each iteration of the IST algorithm consists of gradient step followed by the shrinkage operation. The main advantage of the IST algorithm is that it is very simple. However, the IST algorithm has poor convergence. Several accelerated algorithms were developed such as the Fast Iterative Shrinkage/Thresholding (FIST) algorithm, Two Step Iterative Shrinkage/Thresholding (TwIST) algorithm etc. The TwIST algorithm is explained in the following subsection.

3.2.1 Two Step Iterative Shrinking/Thresholding (TwIST) algorithm

TwIST is the modification of IST and FIST algorithms. The update equation in TwIST depends on the previous two iterations rather than only one iteration. From the Two-Step method for linear systems, a linear function $Ax = B$ is considered where the matrix A is split to C and R given below

$$A = C - R, \tag{3.2}$$

Taking $C = I + \lambda D_i$ and $R = I - \varphi^T\varphi$ in the above equation

$$A = \lambda D_i + \varphi^T\varphi, \tag{3.3}$$

The two-step iteration for linear system $Ax = \varphi^T y$ becomes

$$x_{i+1} = (1-\alpha)x_{i-1} + (\alpha - \beta)x_t + \beta C^{-1}(x_i + \varphi^T(y - \varphi x_i)), \tag{3.4}$$

By setting $\alpha = 1$ and replacing the C^{-1} with shrinkage operator ψ_λ, the Two Step IST is written as

$$x_1 = \Gamma_\lambda(x_0), \tag{3.5}$$

$$x_{i+1} = (1-\alpha)x_{i-1} + (\alpha-\beta)x_i + \beta\Gamma_\lambda(x_i), \tag{3.6}$$

The TwIST algorithm has better converge than IST or FIST algorithms since it updates the equation using the previous two iterations [8]. The pseudo-code of the algorithm is given below.

Two Step Iterative Shrinkage/Thresholding algorithm (TwIST)

Input: $\alpha, \beta, \varphi, y$

Output: x

Consider the linear function: $Ax = B$

A is split to C *and* R: $C = I + \lambda D_i$ and $R = I - \varphi^T\varphi$

Find the value of x_{i+1}:

$$x_{i+1} = (1-\alpha)x_{i-1} + (\alpha-\beta)x_t + \beta C^{-1}(x_i + \varphi^T(y - \varphi x_i))$$

TwIST is performed: $x_1 = \Gamma_\lambda(x_0)$

$$x_{i+1} = (1-\alpha)x_{i-1} + (\alpha-\beta)x_i + \beta\Gamma_\lambda(x_i)$$

α and β values are set: $\alpha = \rho^2 + 1, \beta = \frac{2\alpha}{\xi_m + \xi_1}$

where ρ is given by $\rho = \left(\frac{1-\sqrt{k}}{1+\sqrt{k}}\right) < 1$

3.3 Gradient Projection Algorithms

The gradient projection method was first proposed by Goldstein, Levitin and Polyak [18, 19]. Like IST algorithms, the method requires the matrix vector products

involving φ and φ^T. The gradient projection algorithm is applied to the quadratic formulation in (2.1), where the search path from each iterate is obtained by projecting the negative gradient direction onto a feasible set. This is referred to as the Gradient Projection for Sparse Reconstruction (GPSR). Unlike the Basis Pursuit and l_1 least squares algorithms, GPSR involves only one level of iteration.

GPSR can be solved for a sequence of values of λ in (2.1). Once the solution has been obtained for a specific λ, it can be used as a warm-start for a closer value. It has been noted that the speed of GPSR may degrade considerably for smaller values of the regularization parameter λ. However, if we use GPSR for a larger value of λ, then λ should be decreased in steps towards its desired value [10].

The key step of the GPSR algorithm is to express as a quadratic program by splitting x into its positive and negative parts.

$$x = u - v, u \geq 0, v \geq 0$$

So, the equation (2.1) can be written as a bound constrained quadratic program:

$$\min_{u,v} \frac{1}{2}||y - \varphi(u - v)||_2^2 + \lambda 1_n^T u + \lambda 1_n^T v \quad s.t. \quad u \geq 0, v \geq 0, \tag{3.7}$$

The equation can be written in a more standard format as follows

$$\min_z c^T z + \frac{1}{2} z^T B z \equiv F(z) \quad s.t. \quad z \geq 0, \tag{3.8}$$

where

$$z = \begin{bmatrix} u \\ v \end{bmatrix}, b = \varphi^T y, c = \lambda 1_{2n} + \begin{bmatrix} -b \\ b \end{bmatrix} \; and \; B = \begin{bmatrix} \varphi^T\varphi & -\varphi^T\varphi \\ -\varphi^T\varphi & \varphi^T\varphi \end{bmatrix}$$

The Basic Gradient Projection (GPSR-Basic) algorithm is explained in the following subsection

3.3.1 GPSR-Basic algorithm

Each iteration in the GPSR-Basic search for z^i along the negative gradient $-\nabla F(z^i)$ is projected onto a non-negative orthant [10]. Then, a backtracking line search is performed until a sufficient decrease is attained in F. Here, an initial guess α^i is used that yields the exact minimizer of F along this direction if no bounds were encountered. The vector g^i is defined as follows

$$g_j^i = \begin{cases} (\nabla F(z^i))_j, \ if\ z_j^i > 0\ or\ (\nabla F(z^i))_j < 0, \\ 0, \ otherwise \end{cases} \tag{3.9}$$

The initial guess α^i is chosen

$$\alpha_0 = \arg\min_{\alpha} F(z^i - \alpha g^i), \tag{3.10}$$

To protect the values of α_0 that are too small or large, we confine it to the interval $[\alpha_{min}, \alpha_{max}]$. The pseudo-code of the algorithm is given below.

GPSR-Basic algorithm

Input: $y, \varphi\ and\ \lambda$

Output: x

Initialization: parameters are chosen $\beta \in (0,1)\ and\ \mu\ \in \left(0, \frac{1}{2}\right); set\ i = 0$

Compute the initial guess $\alpha_0 = \frac{\left((g^i)\right)^T g^i}{\left((g^i)\right)^T B g^i}$

Replace α_0 by $mid(\alpha_{min}, \alpha_0, \alpha_{max})$

The backtracking line search is performed

$$F\left(\left(z^i - \alpha^i \nabla F\left(\left(z^i\right)\right)_+\right)\right) \leq F\left(z^i\right) - \mu \nabla F\left(z^i\right)^T (z^i - (z^i - \ \alpha^i \nabla F(z^i))_+)),$$

Set

$$z^{i+1} = z^i - \alpha^i \nabla F((z^i))_+$$

Finally, the convergence test is performed and is terminated with appropriate solution z^{i+1} if it is satisfied.

3.4 Wavelet Based Compression algorithms

The wavelet based compression algorithms incorporate the wavelet tree structure that can be represented by Hidden Markov Tree (HMT). The wavelet coefficients s from (1.1) can be represented in terms of a tree structure for an image. For scale $p = 1$, the coefficients correspond to root nodes and for the large scale $p = L$, the coefficients correspond to leaf nodes. Each wavelet coefficient has four children coefficients, and it has the statistical relationship between parent and children coefficient as shown in the Figure 3. Top left block corresponds to scaling coefficients, which capture the coarse scale representation of an image. These statistics are represented by HMT.

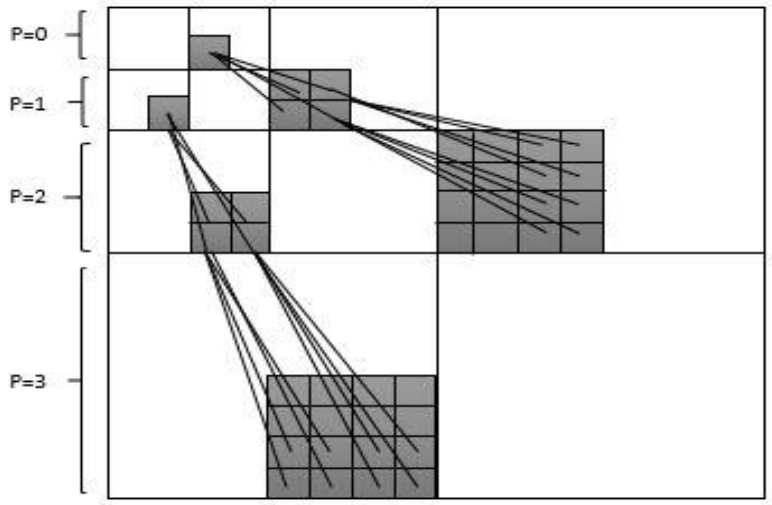

Figure 3. Tree structured wavelet decomposition of an image depicted across scales.

When modelling the statistics by HMT model, the observation is the wavelet coefficient for each of the two states where the observation is drawn from a zero mean Gaussian having low state (low variance) and high state (high variance). In the CS framework, we observe only on the projection of these coefficients, not the wavelet coefficients. If a given parent coefficient is negligible, the children coefficients are also negligible.

Baranuik et al [20] demonstrated that it is possible to improve the performance of compressive imaging reconstruction by introducing independencies between the locations of the image coefficients. A modification of the HMT model was proposed and it is known as Bayesian Compressive Sensing (BCS), where the coefficient associated with low state is set to zero and that infers the coefficients are sparse. Therefore, the Bayesian framework has been employed for the reconstruction of an image and hence the name Bayesian Tree Structured Wavelet – Compressive Sensing (TSW-CS). The Bayesian Compressive Sensing (BCS) framework Matlab code is downloaded from (code available at: http://people.ee.duke.edu/~lcarin/BCS.html).

In addition, it is assumed that all the coefficients at scale p with a zero valued parent share a mixing weight π_p^0. Similarly, all the coefficients at scale p with a non-zero parent share a mixing weight π_p^1. Different Beta priors are imposed based on the scale and the parent coefficients.

3.4.1 Tree Structured Wavelet Compressive Sensing Monte Markov Chain Monte Carlo (TSWCS-MCMC)

The wavelet tree structured information explained in the above section is integrated into the TSW-CS model with a MCMC inference. The two components in the

spike and slab prior, which are used in Bayesian regression models [21] are analogous to the two states (low and high states) in the HMT model. The posterior computation by Markov Chain Monte Carlo (MCMC) has been implemented based on Gibbs sampling (randomized MCMC algorithm that makes use of random numbers and produce different results each time when it is run), where posterior distribution is approximated by sufficient number of samples.

For each MCMC iteration, s can be sampled in a block manner. In block sampling, computing the conditional posterior of s_j uses all other elements of s ($s_k \; for \; k \neq j$) from the last MCMC iteration whereas in sequential sampling, computing the conditional posterior of s_j can use s_k for $k < j$ from current iteration and s_k for $k > j$ from the last iteration [11]. This means, the sequential sampling typically achieves faster convergence i.e., it requires few iterations to achieve MCMC convergence. With the MCMC model, typically a burn-in period of 5000 iterations are required for an image size of 128×128 for image reconstruction with few samples. In addition, the parent-child relationships in the prior setting would provide much sparser solution. The main advantage of TSWCS-MCMC is faster convergence and it outperforms with faster and accurate results when compared to other algorithms such as MP, OMP, TwIST and GPSR etc.

4. Compressive Imaging Configuration and Properties of Light Sources

This chapter describes the physical constructs of compressive imaging setups - the single pixel camera [22] and its modified version [23]. Both classical light (Poisson and thermal light) and nonclassical light (Fock states and squeezed light) are used as the light sources to illuminate the object. The properties of these light sources are described in detail in the following.

4.1 Compressive Sensing (CS) – single pixel camera

One of the main applications of compressive sensing is single pixel camera [22]. The architecture of CS - single pixel camera is comprised of a Digital Micro mirror Device (DMD), two lenses, photon detector and A/D converter. The output image is retrieved from the measurements by the digital computer.

Before going into the working mechanism of CS- single pixel camera, it is important to know the working mechanisms of DMD, and the photon detector. The DMD is a reflective spatial light modulator (SLM) that selectively redirects the light beam. It consists of an array of bacterium sized, electro statistically actuated micro mirrors, where each mirror in the array is suspended above an individual static random access memory (SRAM) cell [22] shown in Figure 4. Each mirror rotates about a hinge and can be positioned in either of the two states +20 and -20 degrees from horizontal. Thus, the light falling on the DMD can be reflected in two directions depending on the mirror orientations.

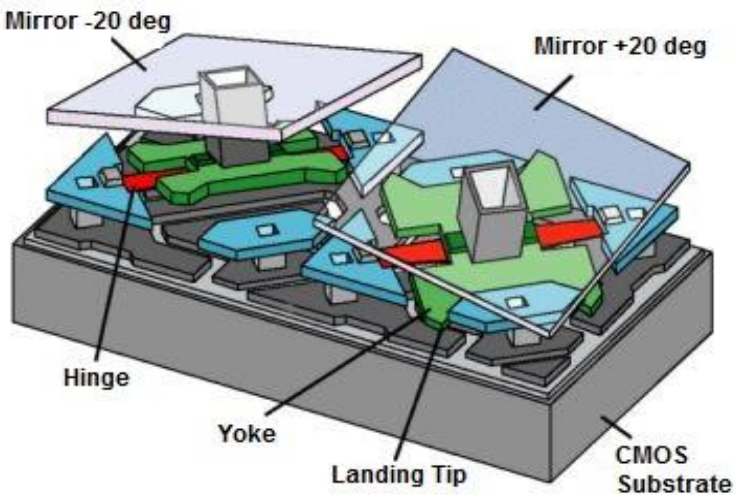

Figure 4. Schematic diagram of DMD (showing orientation of two mirrors) [24]

Generally, the photon detector counts the number of photons in light. It has some surface that absorbs photons and produces voltage effect, which is directly proportional to the absorbed number of photons.

The working mechanism of CS – single pixel camera is (see Figure 5): when a light source illuminates an object, the light is reflected onto the lens 1. From the lens 1, the image is projected onto the DMD that consists of several micro mirrors (each micro mirror represents a pixel of an image and is set to a particular phase). The light is then collected by the lens 2 and focused onto the photon detector. Each mirror can be independently oriented either towards the photon detector or away from the photon detector. Measurements are collected by setting the micro mirror orientations using random number generator in a pseudorandom 0's and 1's pattern (known to be canonical matrix) to create the measurement vector φ. The voltage of the single photo diode is y which is the inner product between measurement matrix φ and the desired image x. This voltage y is digitized by an A/D converter. The process is repeated n

number of times to obtain all entries in y. The design of the camera is very simple and reduces the size. The schematic diagram of a single pixel camera is shown in the figure below

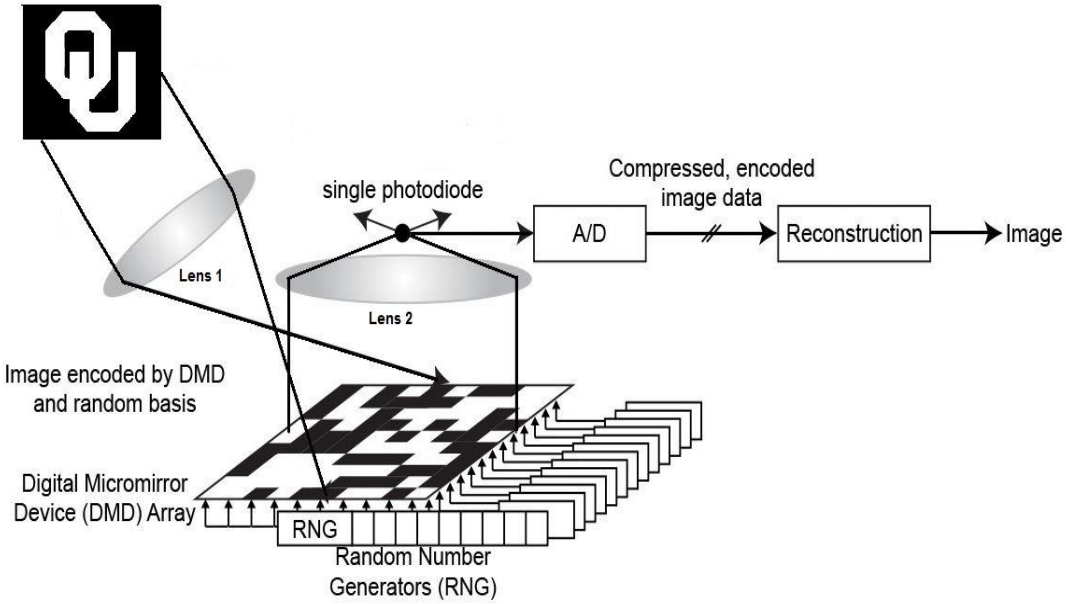

Figure 5. CS - Single Pixel Camera [25]

A modification of CS - single pixel camera is done by introducing DMD's with +1 and -1, where +1 is reflected onto collecting lens 1 and -1 is reflected onto co as shown in the figure 6 [23]. This method uses two photon detectors which collects the photons on both the sides $S_{+1}\ and\ S_{-1}$. The total number of photons collected at the end will be $S = S_{+1} - S_{-1}$. All the measurements are collected by setting the micro mirror orientations using a pseudo random number generator in a pseudo random +1 and -1 pattern (also known for Rademacher distribution).

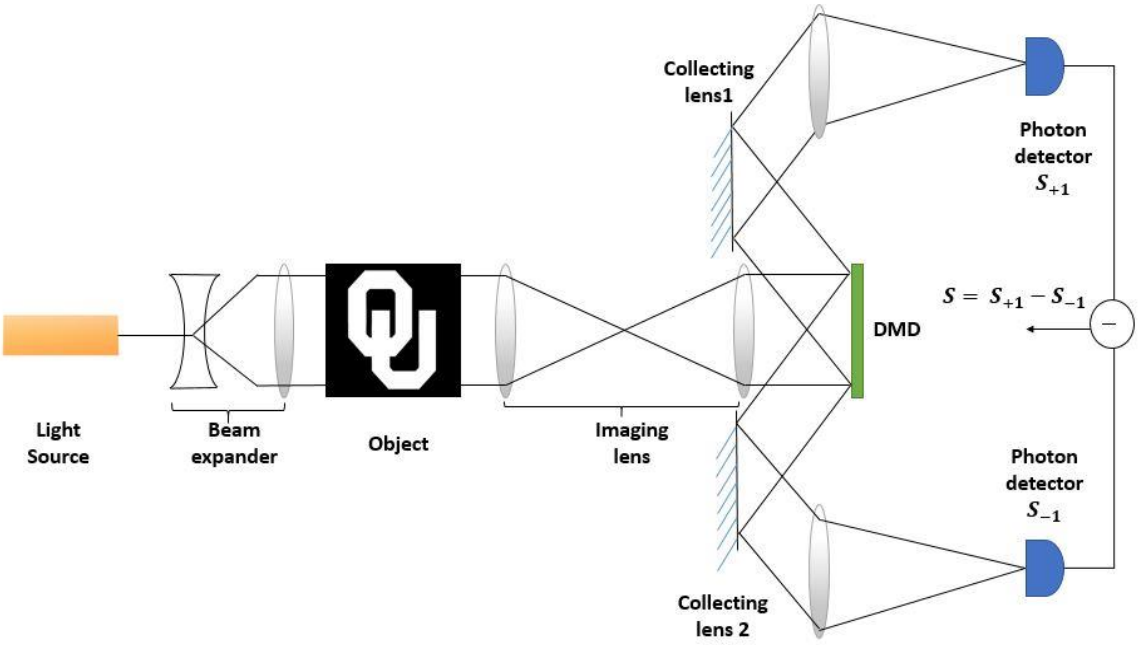

Figure 6. Modified CS – Single Pixel Camera

The advantage of the modified compressive imaging setup is that the use of the Rademacher distribution gives a much better CS reconstruction than 0 and 1 sensing matrix as in the original single-pixel camera. The drawback is the use of an additional photo-detector and the need of a proper synchronization of the output currents from the detectors.

The complete working mechanism can be presented by a mathematical formulation for both noiseless and noisy cases (different light sources such as Gaussian, Fock states, Poisson, thermal, squeezed light) in the following sections.

4.2 Noiseless Case

The mathematical formulation of the noiseless case is mentioned in (1.2) where x is an image that is recovered from noiseless measurements. The noiseless image is independent of the mean photon number. It is easier to compare the mean number of

photons to Root Mean Square Error (RMSE) of two objects, as both noiseless and noisy cases are plotted in a single graph. So is the reason we have considered the noiseless image to be multiplied by the mean photon number. Then the CS optimization algorithms are performed to reconstruct an image from few samples. All the equations mentioned in the Chapter 1 are based on the noiseless case.

From Figure 6, it is assumed that no noise exists and the simulation is done using several CS optimization algorithms.

4.3 Noisy Case

We have considered different light sources such as thermal light, Poisson light, Fock states and squeezed light in the noisy case. The noise here stems from the quantum nature (discreteness) of photons. It is assumed that the detecting system is perfect so that all the noise is arising in the final signal comes solely from the light sources. As a comparison, the usual Gaussian noise is also considered to contrast the behavior of CS in the different cases.

Properties of different light sources are explained in the following subsections.

4.3.1 Gaussian noise

Generally, the Gaussian noise is "added" to the image in the compressive imaging framework according to

$$y = \varphi x + \theta_n, \tag{4.1}$$

where θ_n is the noise added to an image of size $n \times 1$. However, in our simulations we have "applied" Gaussian noise to an image [26]. Generally, Poisson noise is position dependent. This means that noise is accumulated at the position of an object. Since we

are considering zero background gray scale object, we have "applied" Gaussian noise to an image for better comparison between two different objects.

The Gaussian noise usually does not correspond to a real light source of well-defined photon statistics, as the former is a continuous random variable whereas the latter corresponds to a discrete random variable. It is well known that in the limit of very light mean photon number, the Poisson distribution can be approximated by a Gaussian. Nevertheless, the consideration of the Gaussian noise here is for the purpose of comparison, as most CS algorithms assume additive noise of the type of Eq. (4.1), and the main purpose of the thesis is to study the robustness of these algorithms and their behaviors when different noises arising from different photon statistics are considered.

The Gaussian light source has an intensity light distribution given by

$$P_{Gaussian}(I, x|\mu, \sigma) = \frac{1}{\sqrt{2\pi}\,\sigma} e^{-\frac{(I-\mu(x))^2}{2\sigma^2}}, \tag{4.2}$$

where mean = $\mu(x)$ and variance = σ^2.

The Signal-to-Noise ratio (SNR) is given by

$$SNR(x) = \frac{\mu(x)}{\sigma}, \tag{4.3}$$

The Gaussian light source can be used to provide $\mu(x) \gg \sigma$, so that the intensity I has a very low probability of getting negative, which is unphysical. For a binary object, the SNR can be defined without any difficulty when the variance is properly chosen. For an object with a non-unity transmission or reflection coefficient, we need to be careful in defining the SNR.

We consider that the variance is equal to the mean photon number, i.e., $\sigma^2 = \mu$, so that there can be a direct comparison with the Poisson case. To simplify the study, we

also allow the photo detector signal in the Gaussian case to be negative in the low photon regime, while keeping in mind that it is unphysical and is for the purpose of comparison study.

4.4 Photon Statistics of different light sources

Photon statistics can be learned through the statistical distributions produced in the photon counting experiments that use photon detectors to analyze the statistical nature of photons in different light sources such as Fock states, Poisson, thermal and squeezed states.

Suppose the transmission function of the object is $T(x)$ which has the value between 0 and 1. We also consider the light sources having photon statistics $P(n)$ shining uniformly on the object. In this way, the photon statistics of the light passing through the object and measured by the detector [27] can be modelled as

$$P_m(x) = \sum_{n=m}^{\infty} P(n) \frac{n!}{m!(n-m)!} T(x)^m [1 - T(x)]^{n-m}, \quad (4.4)$$

The properties of light sources are described in the following subsections.

4.4.1 Fock states

Fock state corresponds to light with a well-defined number of photons N. It is named after the physicist Vladimir Fock [28]. The photon number distribution is given by $P(n) = \delta_{nN}$. For a binary object $P_m(x) = P(m) = \delta_{mN}$ at the positions with $T(x) = 1$ and $P_m(x) = \delta_{m0}$ at the positions $T(x) = 0$. On the other hand, for an object with a general transmission coefficient,

$$P_m(x) = \frac{N!}{m!(N-m)!} T(x)^m [1 - T(x)]^{N-m}, \quad (4.5)$$

which is a binomial distribution

Fock states are ideal light sources as the variance of photon number is zero. They provide the performance closest to the noiseless situation. Nevertheless, there are no known method to produce them except when the number of photon N is one or two.

4.4.2 Poisson light source

The Poisson light source has Poisson distribution, which models a single mode laser. Poisson noise is generally applied to an image [26]. Adding Poisson noise in compressive imaging framework can be modelled as

$$y \sim Poisson(\varphi x), \tag{4.6}$$

where x is image of interest (to be recovered) and φ is the measurement matrix

For Poisson light source, each pixel in an image (both gray scale image and binary image) will have random number of photons accumulated in it. This means that Poisson noise is correlated with the intensities of an image. Therefore, Poisson noise is position dependent.

The Poisson distribution is given by

$$P(n|\mu) = \frac{e^{-\mu}\mu^n}{n!}, \tag{4.7}$$

where μ is the mean of the distribution

The Poisson distribution has both mean and variance equal i.e., μ

The number of photons hitting the photon detector through the Poisson process is given by

$$P_m(x) = \sum_{n=m}^{\infty} P_{Poisson}(n|\mu) \frac{n!}{m!(n-m)!}\, T(x)^m\, [1 - T(x)]^{n-m}, \tag{4.8}$$

where

$P_{Poisson}(n|\mu)$ is the Poisson distribution

$T(x)^m$ is an image with m number of photons detected

$[1 - T(x)]^{n-m}$ is an image with $n - m$ photons not detected

The above equation (4.8) can be written as

$$P_m(x) = \frac{e^{-T(x)\mu}[T(x)\mu]^m}{m!}, \tag{4.9}$$

The equation (4.9) also follows Poisson distribution having

$$\text{mean} = T(x)\mu$$

$$\text{variance} = T(x)\mu$$

Therefore the signal-to-noise ratio at position x is given by

$$SNR(x) = \sqrt{T(x)\mu}, \tag{4.10}$$

SNR is directly proportional to the square root of the mean number of photons. So, the more the number of photons the better the reconstructed image [29].

4.4.3 Thermal light source

The electromagnetic radiation emitted by a hot body is called thermal light (also known for black-body radiation). The thermal light source has super-Poissonian statistics and is broader than Poisson distribution of Poisson light source [13]. The super-Poissonian statistics are described in detail with the help of Mandel factor Q in the following subsections. The thermal light is noisier that they have large variations in the intensity. In the quantum sense, we can say that they have a large photon number of fluctuations.

The thermal light source possesses photon statistics and the distribution is given by

$$P_{thermal}(n|\mu) = \frac{\mu^n}{(1+\mu)^{n+1}}, \tag{4.11}$$

where mean = μ and variance = $1 + \mu$

The distribution in (4.11) is known as the Bose-Einstein distribution.

Based on the modified CS – Single pixel camera approach, the noisy image illuminated by thermal light is

$$P_m(x) = \sum_{n=m}^{N_{max}} P_{thermal}(n|\mu) \frac{n!}{m!(n-m)!} T(x)^m [1 - T(x)]^{n-m} \quad (4.12)$$

The above equation (3.11) can be written as

$$P_m(x) = \frac{[T(x)\mu]^m}{[1+T(x)\mu]^{m+1}} \quad (4.13)$$

The equation (3.12) also possesses thermal distribution having

$$\text{mean} = T(x)\mu$$

$$\text{variance} = 1 + T(x)\mu$$

From equation (3.12), it is clear that the variance of Bose-Einstein distribution is larger than that of Poisson distribution. Therefore, the signal-to-noise ratio at position x is given by

$$SNR(x) = \sqrt{\frac{T(x)\mu}{1+T(x)\mu}}, \text{ which is always less than or equal to one} \quad (4.14)$$

Thermal light is usually considered when the object sits in an environment with very strong background radiation. As mentioned in the previous subsection (4.4.2) that more the number of photons, better the quality of reconstructed image. Since $SNR \leq 1$, it means that there are only a few photons. This gives sense that the image is noisy and the quality of image reconstructed is poor. In addition, we consider mainly the effect of photons on compressive imaging and ignore the influence of the background excess noise. So is the reason, we are not considering thermal light source in our simulations.

4.4.4 Squeezed multimode

The squeezed light is a special form of light, which possesses sub-Poissonian or super-Poissonian statistics for different squeezing parameter (r), and is researched in

the field of quantum optics [30]. The sub-Poissonian light has a narrower photon number distribution than that of Poisson distribution. This means, it has less noise compared to Poisson and thermal light source. Sub-Poissonian light sits in between Fock states and Poisson Light. One of the main applications of a squeezed light source is to suppress the quantum noise of the photon in high-precision measurement such as the detection of gravitational waves.

In multimode squeezed light, the number of photons accumulated in each pixel is independent of the number of photons in another pixel. That is, we can consider each spatial position of the object be illuminated independently by a squeezed light beam. This is in contrast to single mode squeezed light over the object, in which case the photons arriving at one position of the object are correlated to that on another position of the object.

The photon statistics of squeezed light is given by the following distribution

$$P_{thermal}(n|\alpha, r) = \frac{e^{-\alpha^2(1+\tanh r)}}{\cosh r} \frac{|\tanh r|^n}{2^n n!} \left|H_n\left(\frac{\alpha(1+\tanh r)^2}{\sqrt{2\tanh r}}\right)\right| \quad (4.15)$$

where $H_n(z)$ is the Hermite function of order n

α is related to the light intensity, and

r is the squeezing parameter

We take both α and r to be real numbers. The mean and variance of the photon number of squeezed light is given by

$$\text{mean} = |\alpha|^2 + \sinh^2 r \quad (4.16)$$

$$\text{variance} = 2\sinh^2 r \, cosh^2 r + |\alpha|^2 (coshr - sinhr)^2 \quad (4.17)$$

Based on the modification of CS – single pixel camera, the noisy image illuminated by squeezed light is given as

$$P_m(x) = \sum_{n=m}^{N_{max}} P_{squeezed}(n|\alpha, r) \frac{n!}{m!(n-m)!} T(x)^m [1 - T(x)]^{n-m} \quad (4.18)$$

The statistical distribution of different light sources (Poisson, thermal and squeezed light) are shown in the figure below

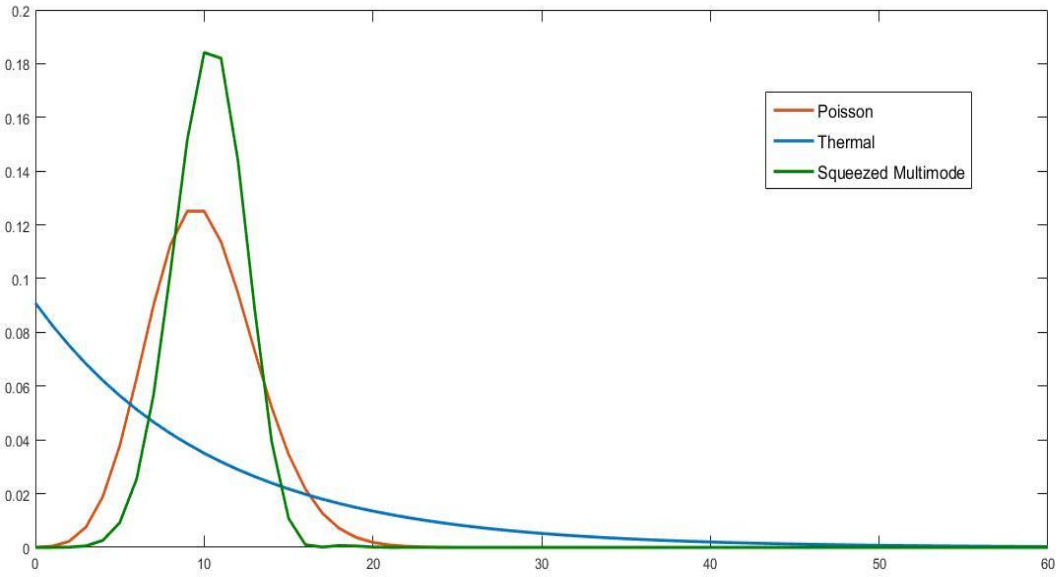

Figure 7. Statistics of different light sources with mean number of photons = 10 and the squeezing parameter (r) = 0.5

4.5 Mandel Factor

L. Mandel introduced the Mandel Q factor in Quantum optics. It is a convenient way to classify the Possionian statistics of light sources. The Mandel Q factor is used to characterize photon count distributions [31] and statistical fluctuations in the number of counts are represented by variance $(\Delta n)^2$.

The mathematical formulation of Mandel Q factor is given by

$$Q = \frac{<(\Delta n)^2> - <n>}{<n>} = \begin{cases} 0 \; for \; Poisson \\ > 0 \quad for \; super - Poissonian \\ < 0 \quad for \; sub - Poissonian \end{cases} \quad (4.19)$$

where n is the photon number

In the squeezed multimode, it possess different statistics for different levels of squeezing parameter r.

5. Simulation results

In this thesis, we have considered two different objects (binary object – OU logo and a gray scale object with zero background) of 128×128 pixels shown in the Figure 4. A gray scale object is an object that has intensities other than 0's and 1's, and the binary object is an object that is comprised of only ones and zeros. These two images are used in the simulation process of different algorithms (MP, OMP, TwIST, GPSR-Basic and TSWCS-MCMC) as described in the Chapter 3.

(a) **(b)**

Figure 8. (a) OU logo – Binary Object (b) Gray scale Object

The results and the observations made from the graphs are explained in this chapter for both binary object and gray scale object.

5.1 Binary Object (OU logo) Results

A log log graph is plotted for different values by taking the Signal-to-Noise ratio (SNR) on x-axis and the Root Mean Square Error (RMSE) on y-axis. We have considered the mean photon number varying from 0 to 1000, as SNR is directly proportional to the square root of the mean number of photons (Gaussian and Poisson case) and SNR is dependent on the mean photon number and the squeezing parameter 'r'. RMSE is the root MSE between original image and the reconstructed image. We

have set the scale of x-axis from 0.4 to 70 and the scale of y-axis from 0.0008 to 3. The graph is plotted for different algorithms (MP, OMP, TwIST, GPSR and TSWCS-MCMC) by considering different light sources (Gaussian, Poisson and squeezed light). In addition, the noiseless case is also plotted in the same graph for different algorithms in the same graph. The RMSE values of noiseless case of OMP and TSWCS-MCMC are not displayed, as their RMSE values are below the defined y-axis scale. The graph is shown below.

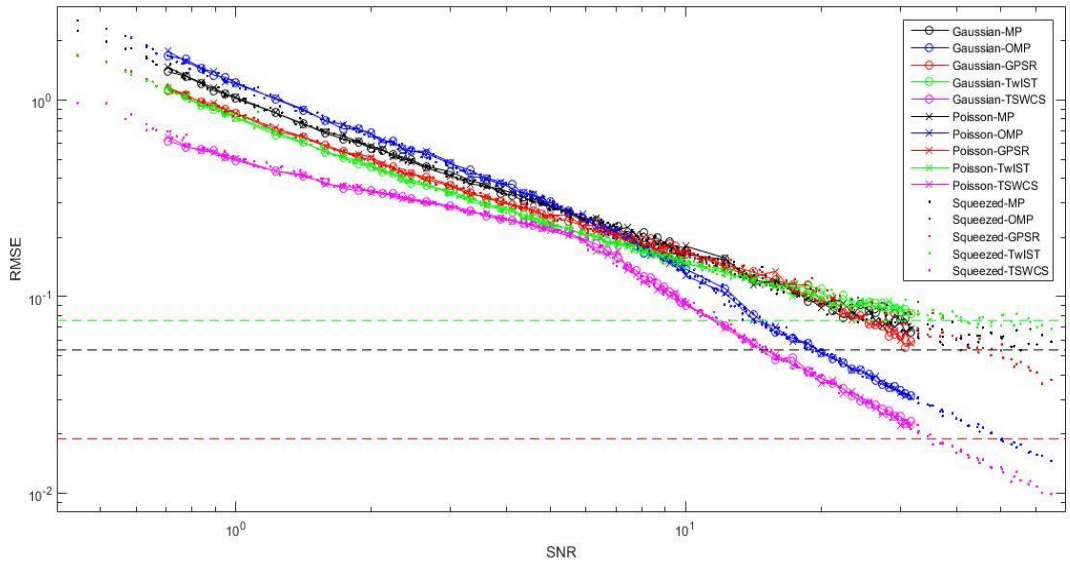

Figure 9. Comparative analysis of different algorithms by considering different light sources for a binary OU logo object (SNR Vs RMSE).

The binary object (OU logo) in Figure 8(a) is restored from only $\frac{1}{4}$ samples (i.e., 25% of 16384 samples).

The valuable observations made from the graph are:

1. The common observation is that, higher the SNR, better the reconstructed image quality (i.e., low RMSE).

2. Gaussian (represented by ‘o’) and Poisson noise (represented by ‘x’) perform almost the same way for all the algorithms.
3. In the case of squeezed light (represented by ‘.’), we have considered $r \in [0.1,1.5]$. As SNR depends on the mean photon number and squeezing parameter in squeezed light, we see that some dotted points are plotted for SNR beyond the value SNR ≅ 33. In addition, the graph shows that the squeezed light performs almost the same as with Gaussian and Poisson for all the algorithms. Note that, we did not differentiate several values of r in the above graph.
4. The RMSE values of MP (represented by the black line), GPSR (represented by the red line) and TwIST (represented by the green line) algorithms ‘decrease linearly’ with increase in SNR. There comes a point beyond SNR ≅ 33, where the RMSE values become saturated.
5. The RMSE values of OMP (represented by blue line) algorithm decrease linearly till certain point SNR ≅ 8, and then there is a steep decrease in the RMSE values beyond SNR ≅ 8.
6. The RMSE values of TSWCS-MCMC (represented by magenta line) algorithm shows better results compared to other algorithms in low photon regime. Its RMSE values decrease linearly until a certain point SNR ≅ 5, and then there is steep decrease in the RMSE values beyond SNR ≅ 5.

As we have already mentioned the larger the SNR, the better the image quality (low RMSE). This means that all the algorithms should have linear decrease in the RMSE values with increase in SNR. However, two algorithms i.e., OMP and TSWCS-MCMC stand out, as their plot does not linearly decrease with an increase in SNR.

The following graphs show the log log plot between the mean number of photons 'n' and RMSE for different values of squeezing parameter 'r' for each algorithm.

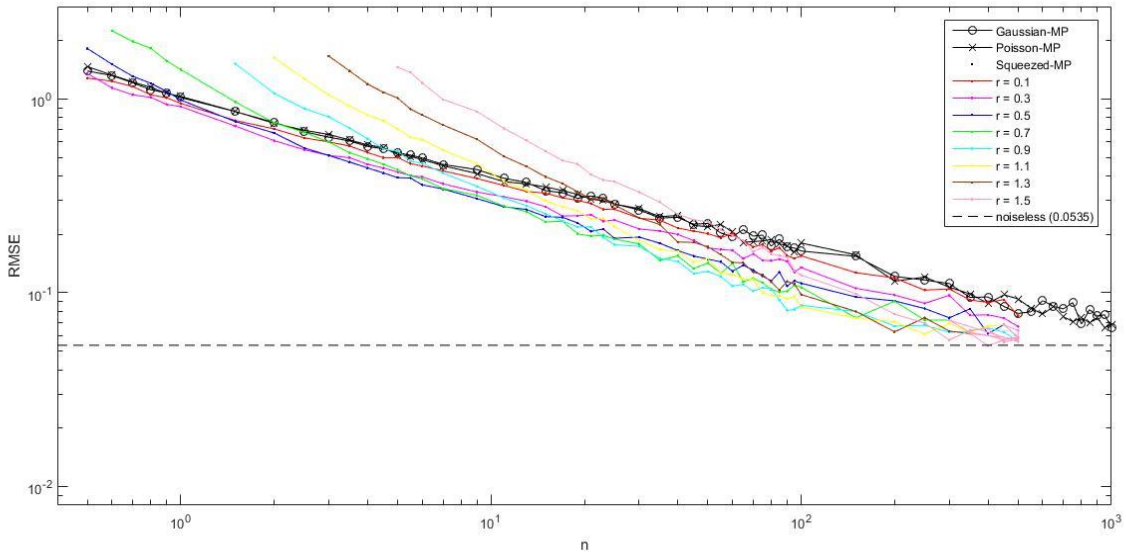

(a) MP algorithm with different light sources

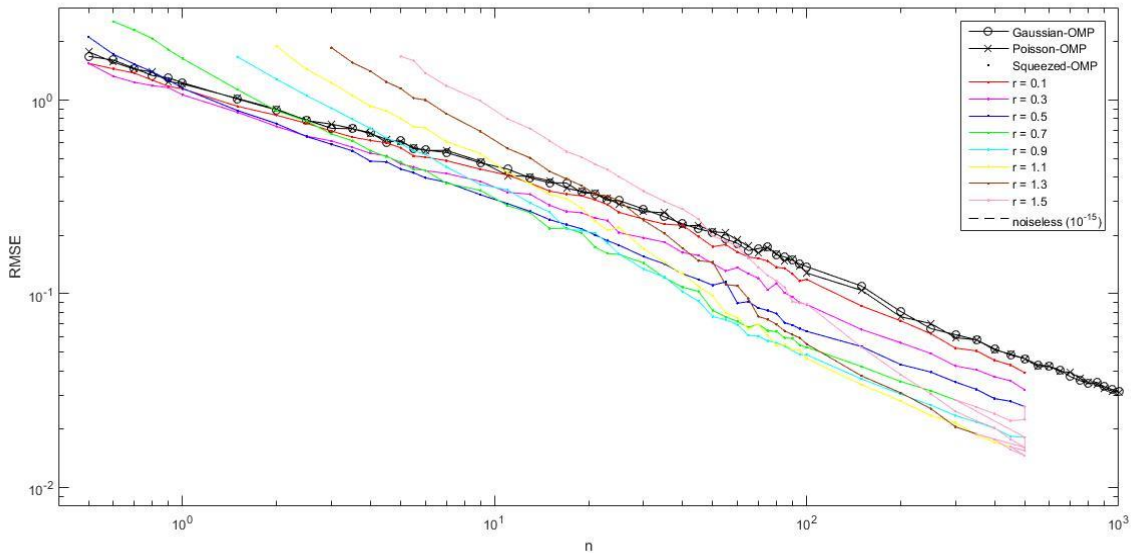

(b) OMP algorithm with different light sources

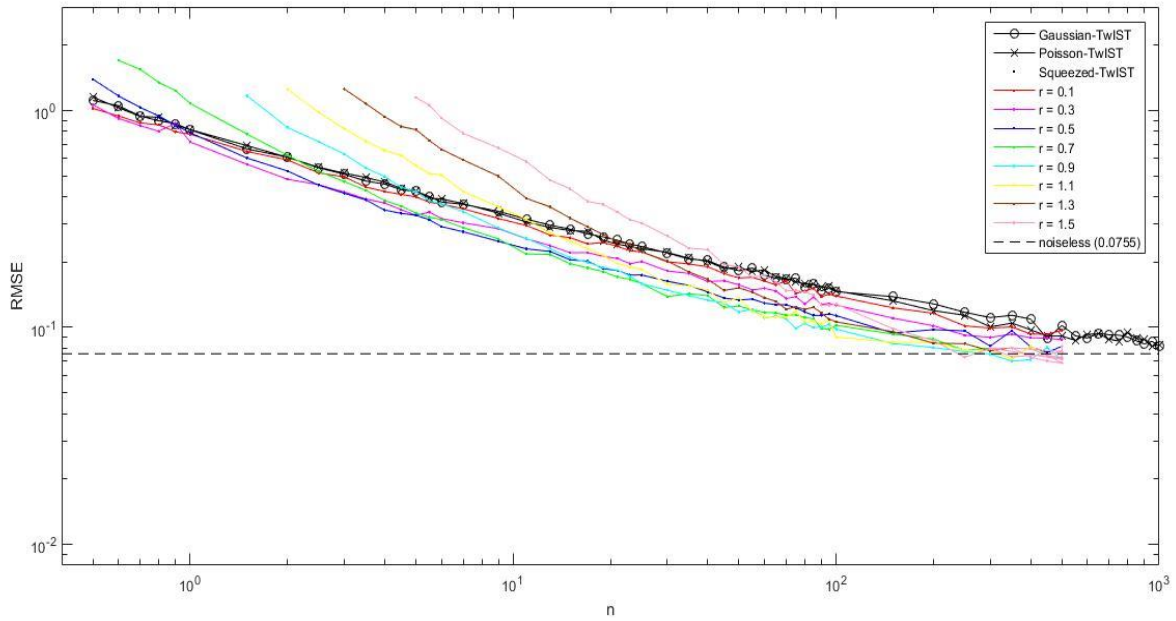

(c) TwIST algorithm with different light sources

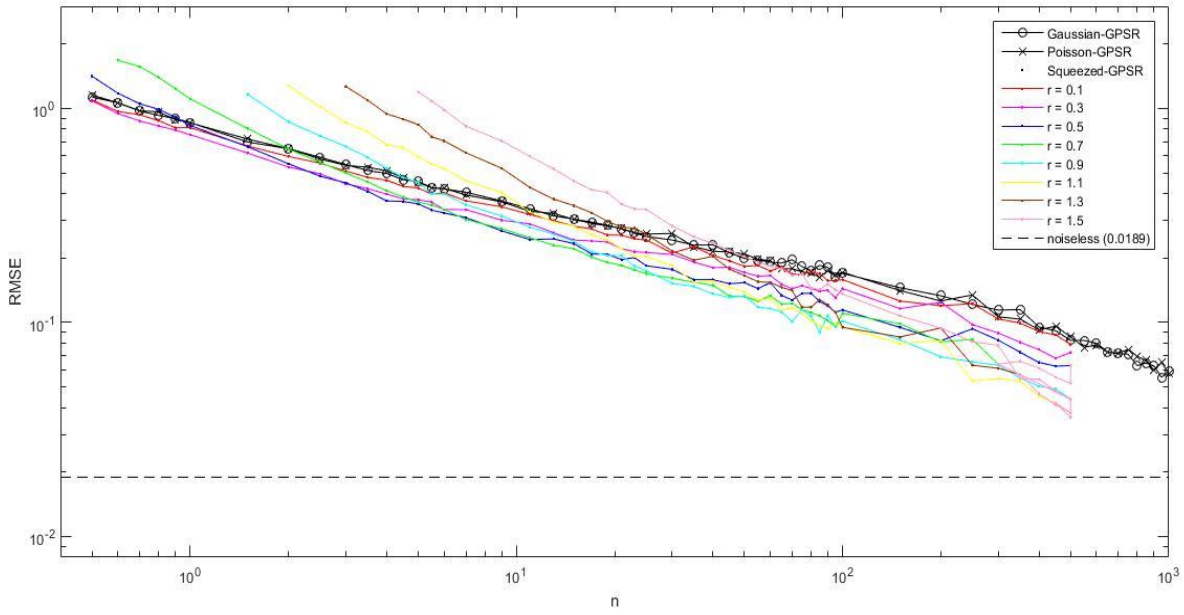

(d) GPSR algorithm with different light sources

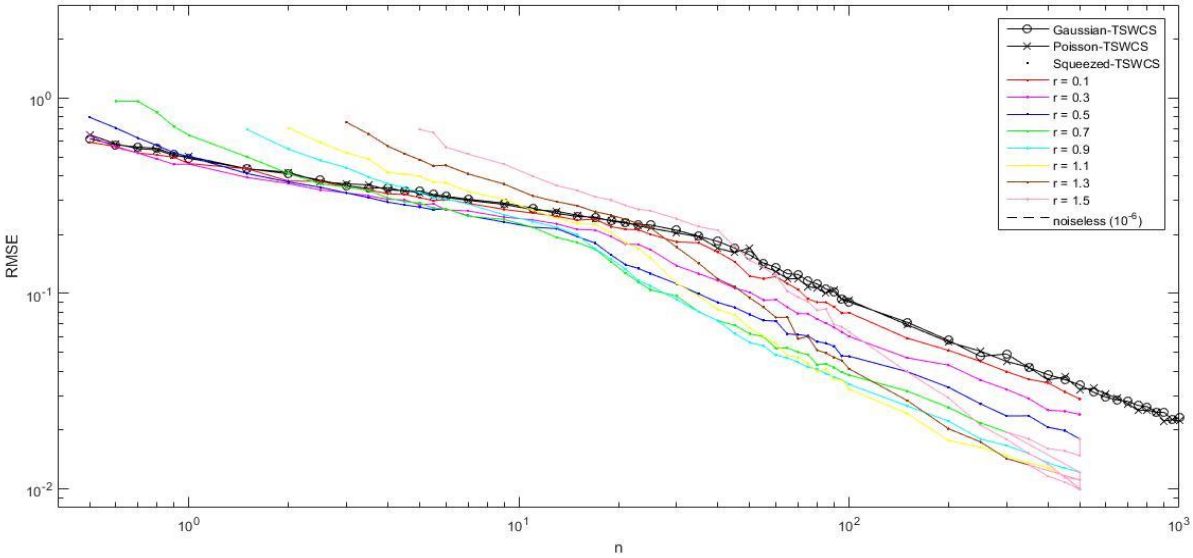

(e) TSWCS-MCMC algorithm with different light sources

Figure 10. (a), (b), (c), (d) and (e) are plots of each algorithm by considering light sources (number of photons 'n' Vs RMSE)

To understand clearly the comparative analysis, we have considered log log plot between photon number 'n' and RMSE for each algorithm.

The observations made from Figure 10 are:

1. Gaussian and Poisson noise perform almost the same and it linearly decreases with increase in the number of photons for MP, TwIST and GPSR algorithms. For OMP algorithm, the RMSE values decrease linearly until a certain photon number and deviates slightly continuing linear decrease with increase in the photon number. For the TSWCS-MCMC algorithm, the RMSE values decrease linearly until a certain photon number and there is a steep decrease in RMSE values with an increase in the photon number.
2. In the case of squeezed light, we have differentiated the squeezing parameter 'r' with different colors.

a. For MP and TwIST algorithms, all the different squeezing parameters ($r = 0.1, 0.3, 0.5, 0.7, 0.9, 1.1, 1.3\ and\ 1.5$) decrease linearly until a certain photon number and becomes saturated with increase in the photon number.
b. For GPSR algorithm, all the different squeezing parameters decrease linearly with increase in the photon number.
c. For OMP and TSWCS-MCMC algorithms, all the different squeezing parameters decrease linearly until a certain photon number and there is steep decrease in the RMSE values with an increase in the photon number.

3. For higher squeezing parameter i.e., $r = 0.5, 0.7, 0.9, 1.1, 1.3, 1.5$ and high photon number, the RMSE values are low. This means that higher the squeezing and high photon number, the better the quality of reconstructed image.
4. Since this thesis deals mostly in low photon regime, for low squeezing parameter $r = 0.1, 0.3$ and low photon number, the RMSE values are low. The higher squeezing parameters do not perform well in the low photon regime.
5. All the graphs have RMSE values of the squeezing parameter above and below the Poisson noise. For the Poisson noise, we know that variance is equal to mean. From the calculations of variance, we see that the RMSE values of different squeezing parameters above Poisson noise comes under super-Poissonian and the values below the Poisson noise are sub-Poissonian.

As mentioned earlier, all the images are reconstructed with ¼ of samples. We have a huge amount of data plotted (shown in the Figures 9, 10) for different levels of SNR. In this thesis, we show the reconstructed images in low photon, low-mid level, and high photon case for Gaussian noise, Poisson noise and squeezed light. The results of the

reconstructed image are shown for different algorithms and for different light sources in the following

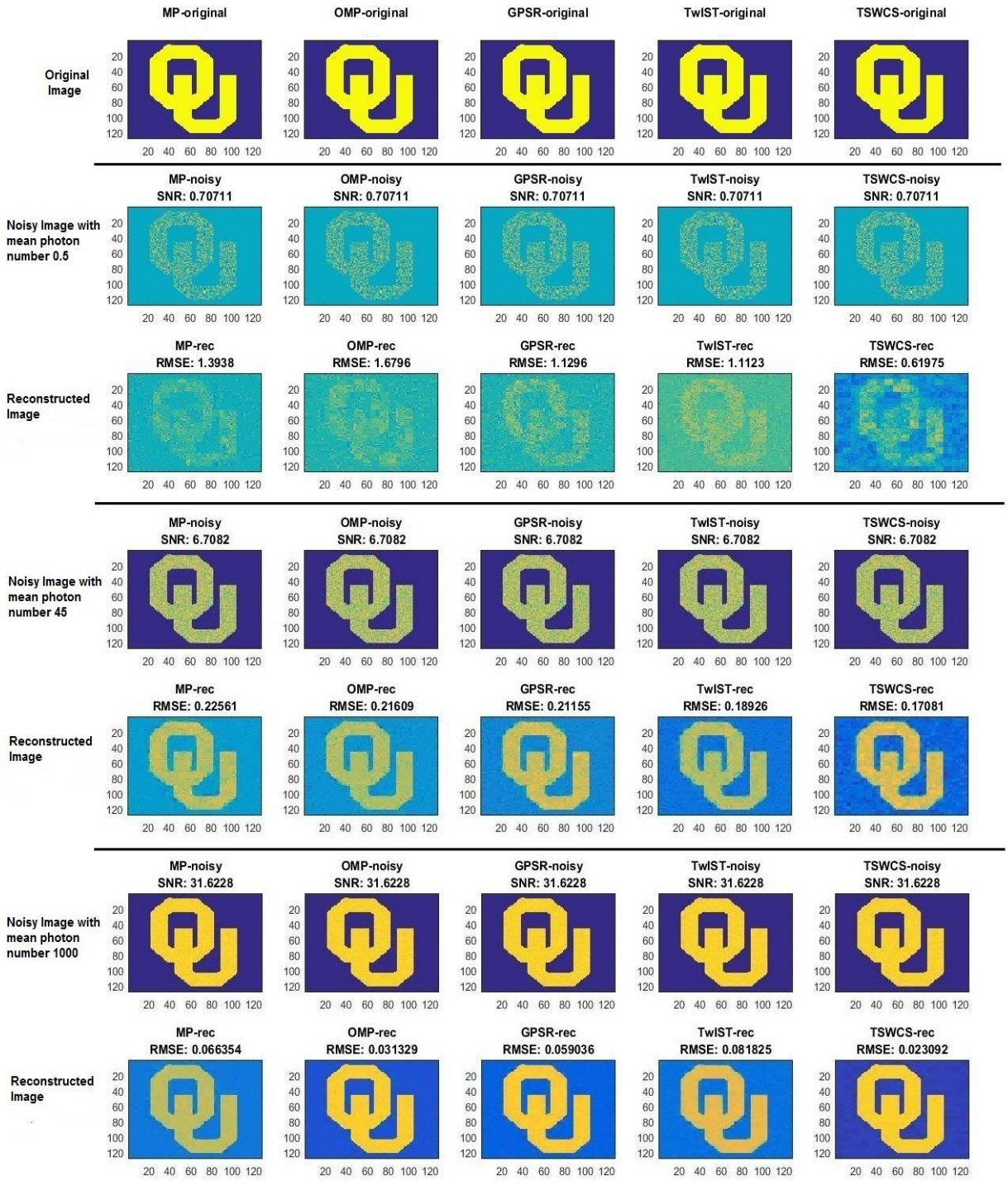

Figure 11. OU logo reconstructed with ¼ samples having mean photon number of 0.5, 45 and 1000 respectively in the presence of Gaussian noise

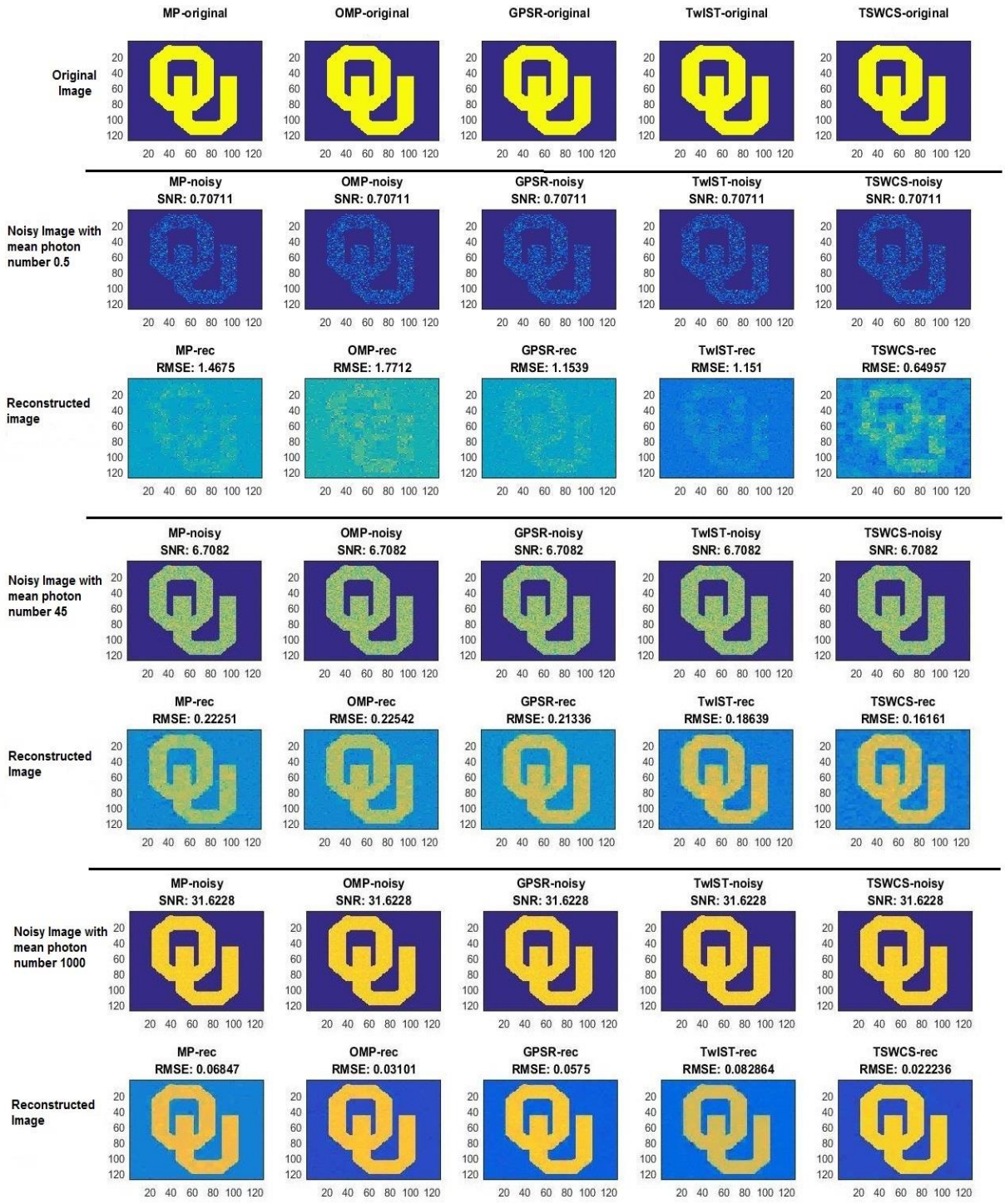

Figure 12. OU logo reconstructed with ¼ samples having mean photon number of 0.5, 45 and 1000 respectively in the presence of Poisson noise

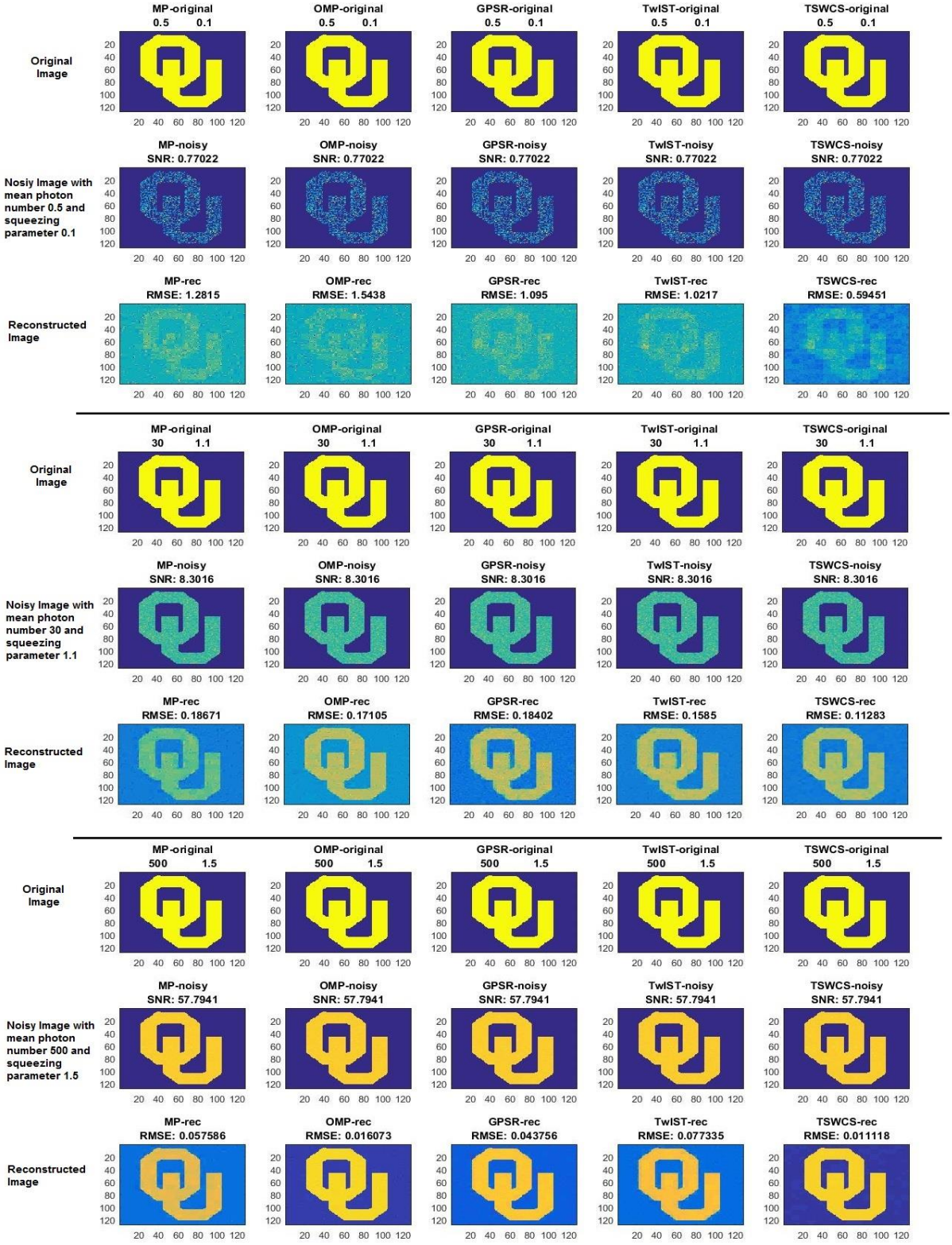

Figure 13. OU logo reconstructed with ¼ samples having mean photon number 0.5, 30 and 500 respectively for the given squeezed light source

From Figure 11, we see that the OU logo image is reconstructed with ¼ samples for different algorithms in the presence of Gaussian noise. The TSWC-MCMC algorithm performs far better than all other algorithms in terms of low RMSE and has a better-reconstructed image quality in low, low-mid level and high photon regime.

Another interesting observation is that, some algorithms such as OMP, GPSR algorithms perform well in the high photon regime compared to other algorithms. These algorithms do not perform well in low photon regime compared to other algorithms. TwIST algorithm shows good performance in low photon regime compared to all other algorithms. The quality of image reconstructed in high photon regime is not good if compared to other algorithms.

From Figure 12, it is clear that TSWCS-MCMC algorithm out performs all other algorithms in terms of better image quality in low, low-mid level and high photon regime.

In the higher photon regime, some algorithms such as OMP, GPSR perform well in terms of low RMSE. The same algorithms do not give better results in low photon regime. TwIST algorithm performs well in low photon regime in terms of image quality and low RMSE.

Figure 13 shows the results of a reconstructed image for the mean photon number 0.5, 30, and 500 for squeezing parameters 0.1, 1.1 and 1.5 respectively. For the squeezed light source, the SNR depends on the mean photon number and the squeezing parameter 'r'. It is also clear that TSWCS-MCMC algorithms outperforms all other algorithms in terms of image quality and low RMSE.

5.2 Gray scale Object Results

The size of the gray scale object is 128×128 pixels. Similar to OU logo image, the gray scale object is reconstructed from ¼ samples. All the data is log log plotted for different values of average SNR vs RMSE. Since the gray scale object has values varying from zero to 255, defining a SNR is difficult. Therefore, we have considered average SNR. We have set the scale of x-axis from 0.4 to 70 and the scale of y-axis from 0.0008 to 3. The plots are shown in the following

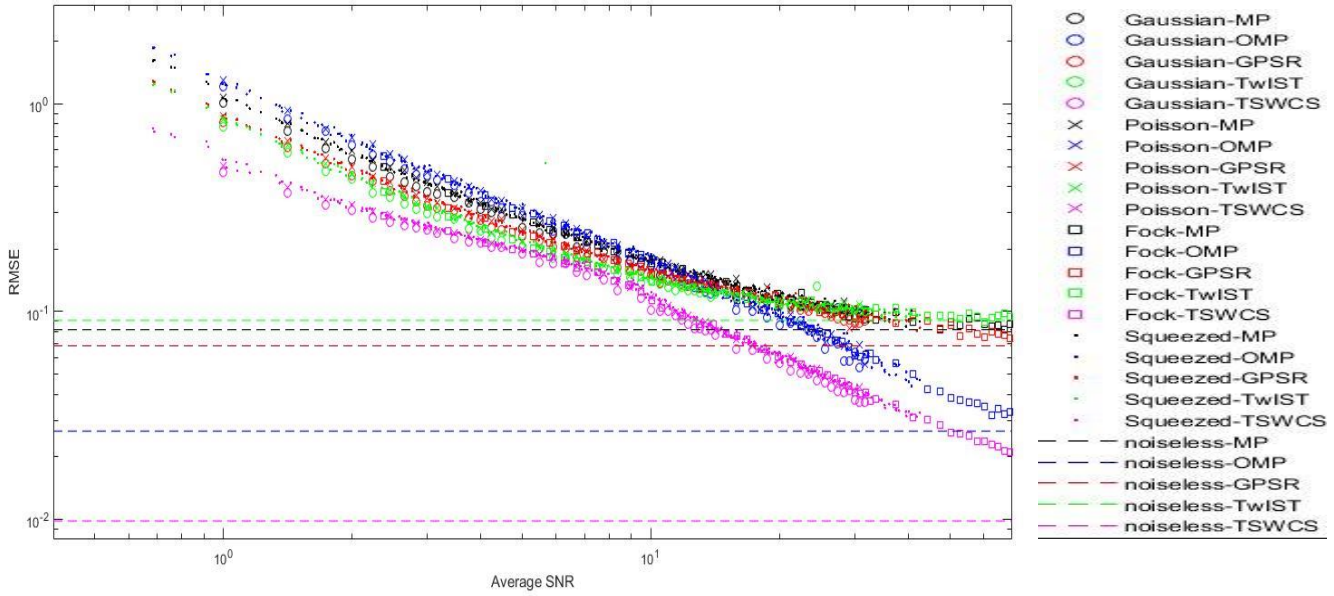

Figure 14. Comparative analysis of different algorithms by considering different light sources for a gray scale object (SNR Vs RMSE).

Before going into observations, the average SNR can be calculated as follows

The mean photon number $\langle N \rangle$ of light source is given by $\sum_n P_n n \equiv \bar{n}$, (5.1)

The variance $\langle \Delta^2 N \rangle$ is given by

$$\left(\overline{n^2}\frac{\langle T^2\rangle}{\langle T\rangle} - \bar{n}^2\frac{\langle T^2\rangle}{\langle T\rangle}\right) + \bar{n}\left(1 - \frac{\langle T^2\rangle}{\langle T\rangle}\right), \quad (5.2)$$

Where $\langle T \rangle = \sum_x T_x$

$$\langle T^2 \rangle = \sum_x T_x^2$$

For binary object (OU logo), $\langle T \rangle = \langle T^2 \rangle$

The average SNR is given as

$$avg\langle SNR \rangle \equiv \frac{\langle N \rangle}{\sqrt{\langle \Delta^2 N \rangle}} = \frac{\bar{n}}{\sqrt{\left(\overline{n^2}\frac{\langle T^2 \rangle}{\langle T \rangle} - \bar{n}^2\frac{\langle T^2 \rangle}{\langle T \rangle}\right) + \bar{n}\left(1 - \frac{\langle T^2 \rangle}{\langle T \rangle}\right)}}, \tag{5.3}$$

where $\overline{n^2} \equiv \Delta^2 n + \bar{n}^2$

The above equation can be simplified as

$$avg\langle SNR \rangle = \frac{\bar{n}}{\sqrt{\left(\Delta^2 n\frac{\langle T^2 \rangle}{\langle T \rangle}\right) + \bar{n}\left(1 - \frac{\langle T^2 \rangle}{\langle T \rangle}\right)}}, \tag{5.4}$$

where $\Delta^2 n$ is the variance of photon number of light sources

The valuable observations made from the graph in Figure 14 are:

1. The common observation is that, higher the average SNR, the better the reconstructed image quality (i.e., low RMSE).
2. Gaussian (represented by ‘o’), Poisson noise (represented by ‘x’) and Fock state (represented by ‘square’) perform almost the same way for all the algorithms.
3. In the case of squeezed light (represented by ‘.’), we have considered $r \in [0.1, 0.3, 0.5, 0.7, 0.9, 1.1, 1.3, 1.5]$. As average SNR depends on the mean photon number and squeezing parameter in squeezed light, we see that some dotted points are plotted for average SNR beyond the value of average SNR ≅ 33. In addition, the graph shows that the squeezed light performs almost the same as with Gaussian, Poisson and Fock for all the algorithms. Note that, we did not differentiate several values of r in the above graph.

4. The RMSE values of MP (represented by black color), GPSR (represented by red color) and TwIST (represented by green color) algorithms ‘decrease linearly’ with increase in average SNR. There comes a point beyond average SNR ≅ 33, where the RMSE values become saturated.
5. The RMSE values of OMP (represented by blue color) algorithm decrease linearly until a certain point of average SNR ≅ 12, and then there is steep decrease in the RMSE values beyond average SNR ≅ 12 with increase in average SNR.
6. The RMSE values of TSWCS-MCMC (represented by magenta color) algorithm show better results compared to other algorithms in low photon regime. Its RMSE values decrease linearly until a certain point average SNR ≅ 9, and then there is a steep decrease in the RMSE values beyond average SNR ≅ 9 with increase in average SNR.
7. Since all the algorithms mentioned in this thesis are designed for Gaussian noise model, the Gaussian noise perform well in terms of low RMSE compared to other noise cases for gray scale object.

As we have already mentioned that higher the average SNR, the better the image quality (low RMSE). This means that all the algorithms should have linear decrease in the RMSE values with increase in average SNR. However, two algorithms i.e., OMP and TSWCS-MCMC stand out, as their plot is not linearly decreasing with increase in average SNR.

For a particular mean photon number in squeezed light case, the SNR value varies with the squeezing parameter i.e., SNR increases with increase in the squeezing

parameter until a certain point in the squeezing parameter data set and then the SNR decreases beyond that squeezing parameter. This means that the RMSE decreases with increase in squeezing parameter until a certain point and then the RMSE value increase beyond that squeezing parameter.

The results of reconstructed image (in low, low-mid level, high photon regime) are shown for different algorithms and for different light sources in the following

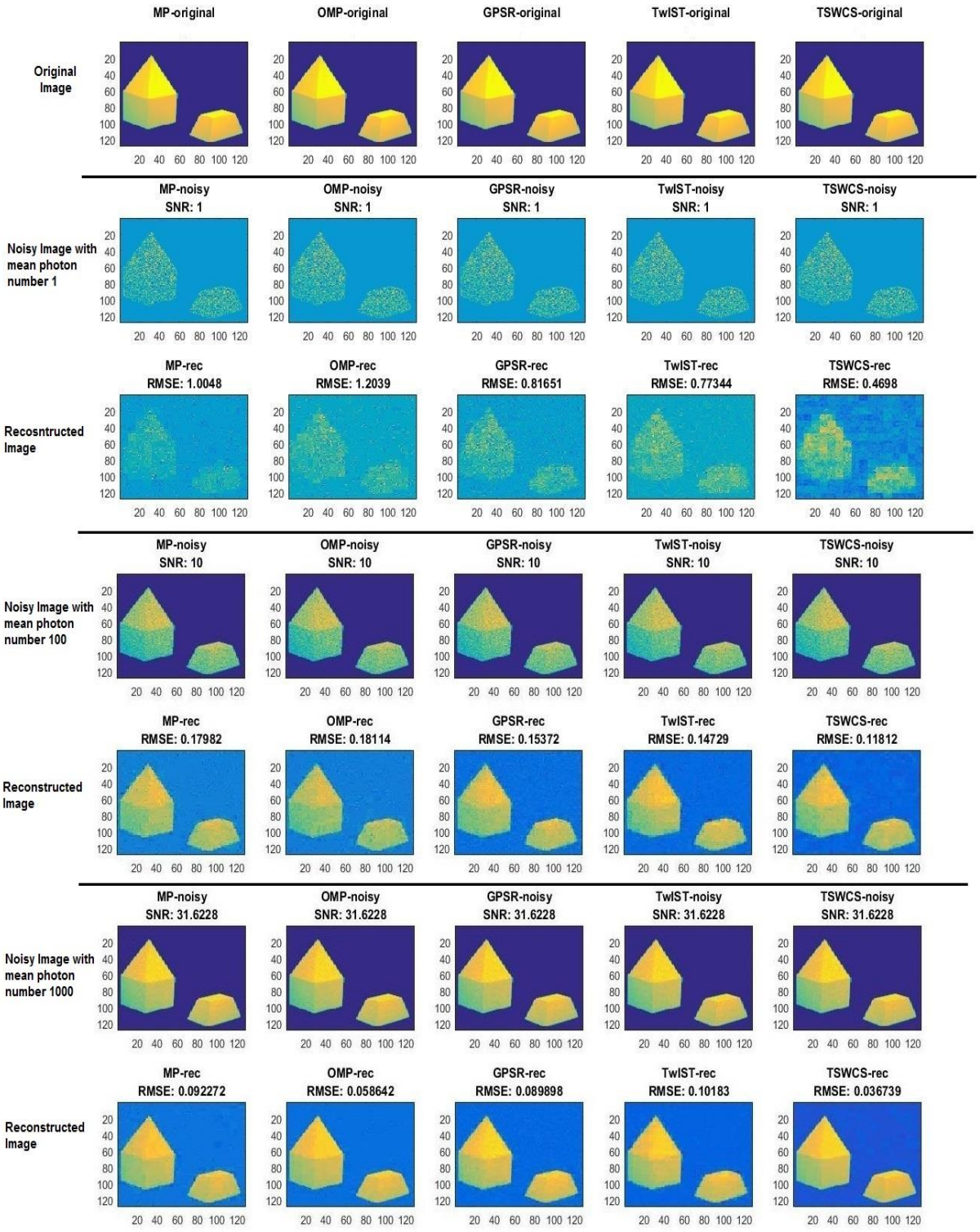

Figure 15. Gray scale object reconstructed with ¼ samples having mean photon number 1, 100 and 1000 respectively in the presence of Gaussian noise

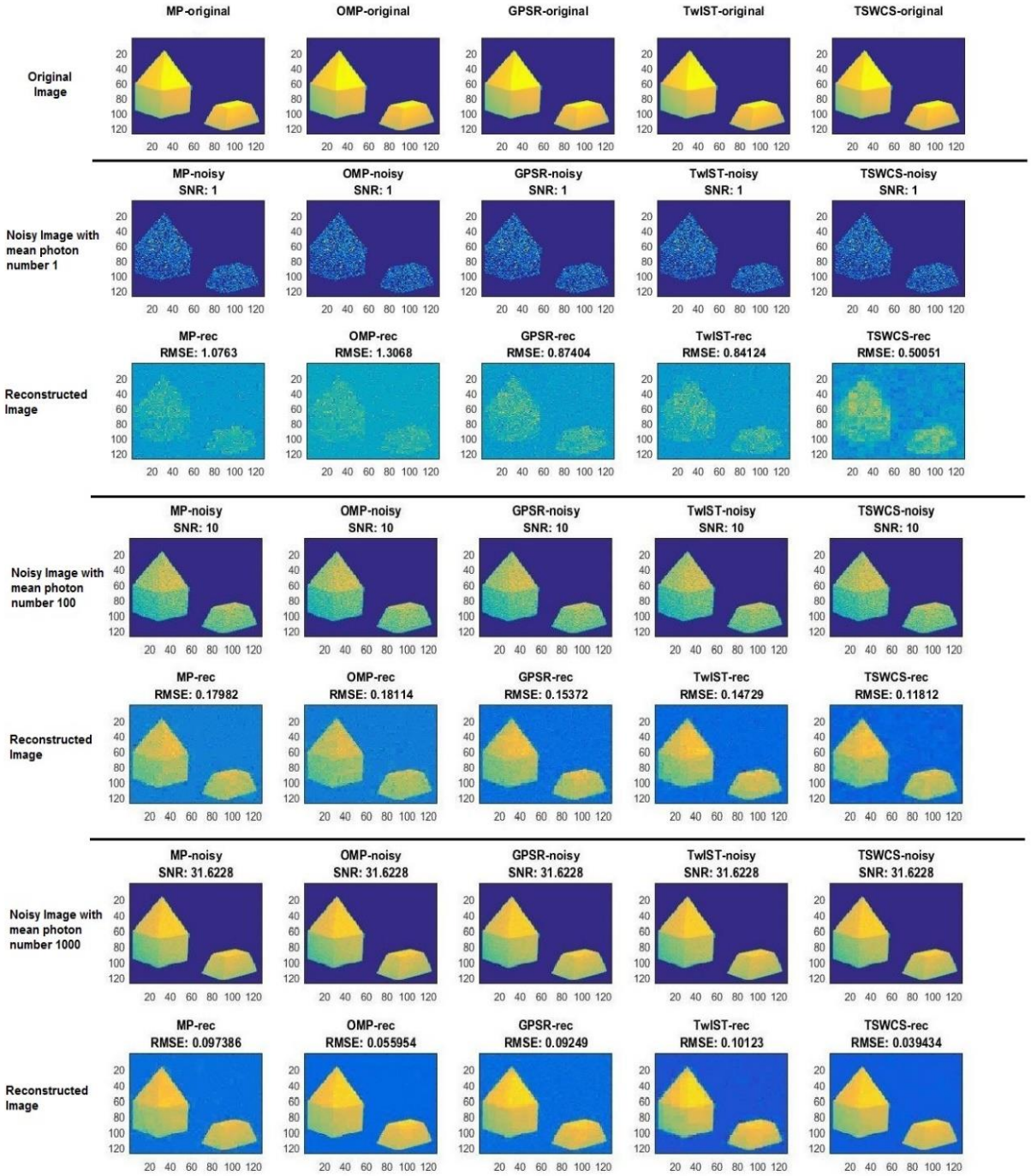

Figure 16. Gray scale object reconstructed with ¼ samples having mean photon number 1, 100 and 1000 respectively in the presence of Poisson noise

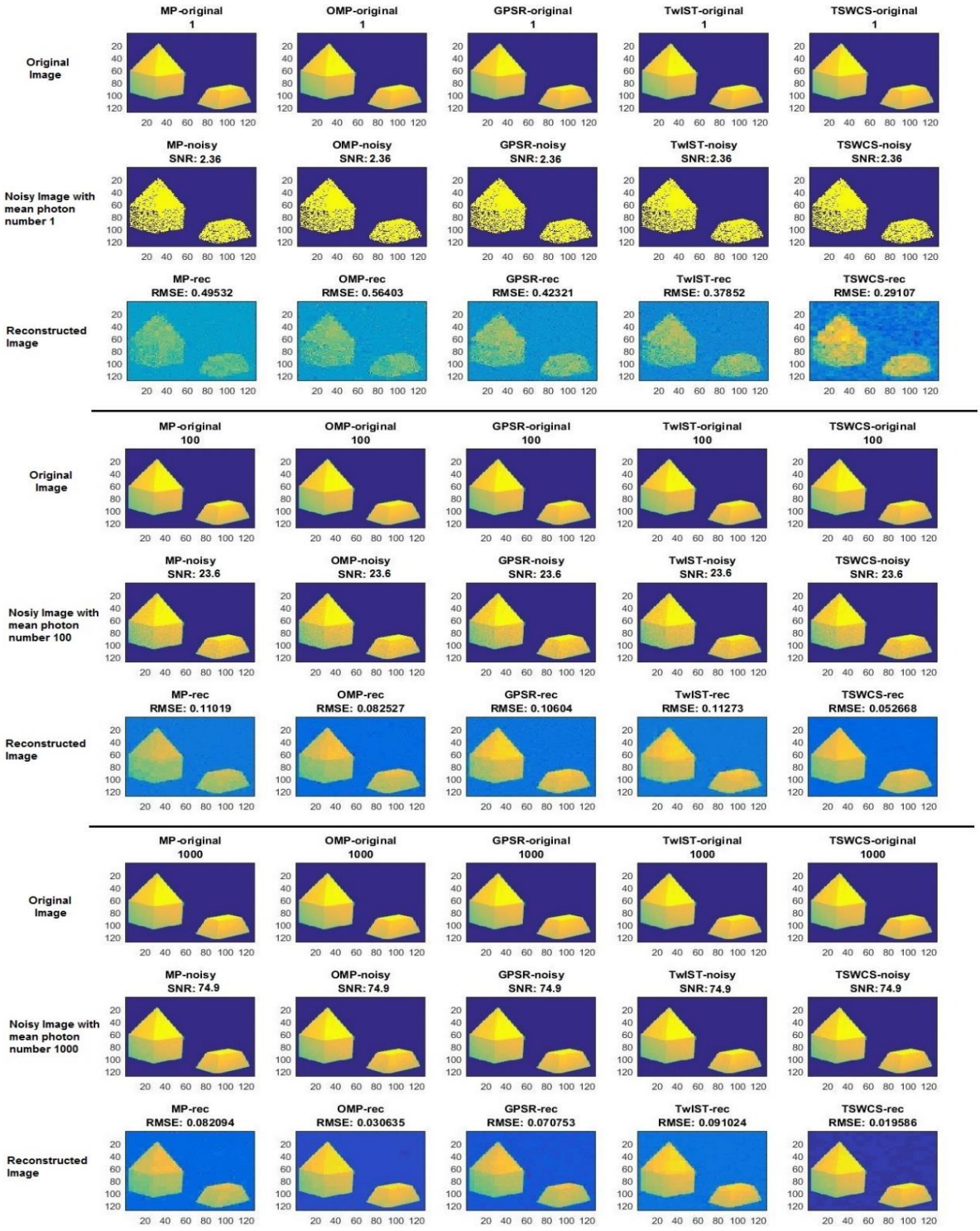

Figure 17. Gray scale object reconstructed with ¼ samples having mean photon number 1, 100 and 1000 respectively for Fock states.

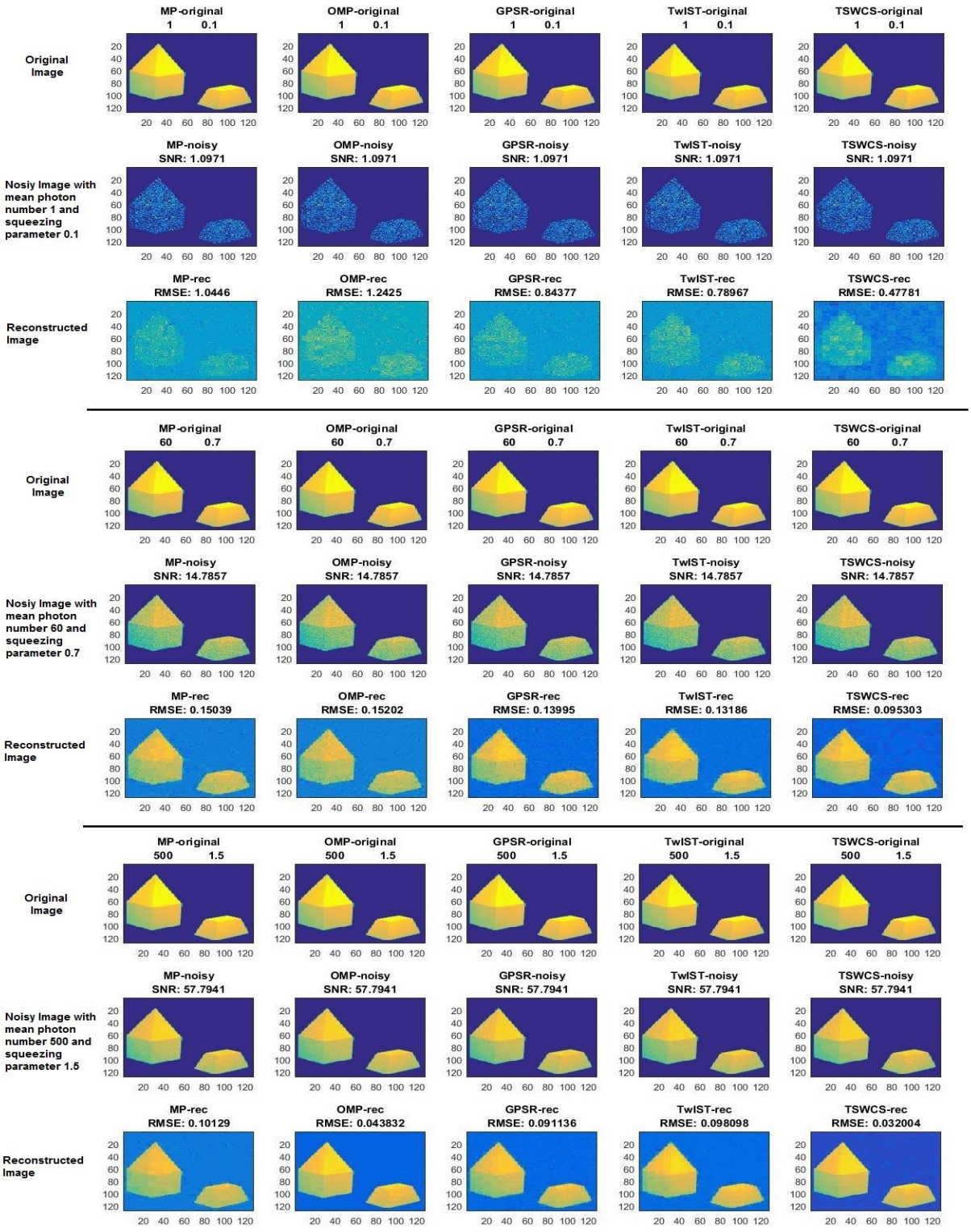

Figure 18. Gray scale object reconstructed with ¼ samples having mean photon 1, 60 and 500 respectively for the given squeezed light source

6. Conclusions and Future work

6.1 Conclusion

In this thesis, we have described CS recovery algorithms (Greedy, Thresholding and Bayesian algorithms) in the presence of different light sources (Fock, Gaussian, Poisson and squeezed light) by considering their photon statistics. We have not considered Thermal noise, as its SNR is always less than 1 (higher noise level). The simulated results were obtained for the two different images (OU logo and Indorre), that are reconstructed with ¼ samples (less than Nyquist rate).

The modified single pixel camera setup having two photon detectors (see Figure 6) is implemented in a simulated environment to reconstruct an image with less number of samples. Since the image size is 128×128 pixels, the computational time required for reconstructing an image for different SNR levels for GPSR and TSWCS-MCMC algorithms is larger than other algorithms. Though the computational time is larger for GPSR and TSWCS-MCMC algorithms, they are especially good for image reconstruction (very low RMSE) without addition of noise.

Generally, the higher the number of photons, the better the reconstructed image quality. This means that the RMSE values have power law with number of photons. From the results in figure 9 and 14, we see that two algorithms (OMP and TSWCS-MCMC) differ linearity compared to other algorithms.

In the case of squeezed light, we know that SNR depends on the mean photon number and the squeezing parameter. For a particular mean photon number, the SNR value varies with the squeezing parameter i.e., SNR increases with increase in the squeezing parameter until a certain point in the squeezing parameter data set and then

the SNR decreases beyond that squeezing parameter. This means that the RMSE decreases with increase in squeezing parameter until a certain point and then the RMSE value increase beyond that squeezing parameter.

In a low photon regime, we see that the detection of binary and gray scale object are almost similar in the presence of noise.

6.2 Future Work

In this thesis, we have used modified CS- single pixel camera in the simulation environment by taking Rademacher distribution (+1 and -1) for sensing matrix. The immediate future work is to implement different light sources in Bayesian framework of compressive sensing etc. In addition, the expander graphs for sensing matrix are considered for different light sources for comparative analysis.

As we know, many CS recovery algorithms are designed by considering Gaussian noise model. The Matlab codes for CS recovery algorithms can be downloaded from https://sites.google.com/site/igorcarron2/cs#reconstruction. However, many applications consist of counting of discrete events, which cannot be modelled using Gaussian noise model. Instead, the Poisson noise model is required. The results obtained for different light sources by studying photon statistics would help in designing generalized compressive imaging framework that incorporates photon statistics.

References

[1] E. J. Candè and M. B. Wakin, "An introduction to compressive sampling," *Signal Processing Magazine, IEEE,* vol. 25, pp. 21-30, 2008.

[2] D. L. Donoho, "Compressed sensing," *Information Theory, IEEE Transactions on,* vol. 52, pp. 1289-1306, 2006.

[3] P. Zerom, K. W. C. Chan, J. C. Howell, and R. W. Boyd, "Entangled-photon compressive ghost imaging," *Physical Review A,* vol. 84, p. 061804, 2011.

[4] O. Katz, Y. Bromberg, and Y. Silberberg, "Compressive ghost imaging," *Applied Physics Letters,* vol. 95, p. 131110, 2009.

[5] D. Ma, Z. Yu, J. Yu, and W. Pang, "A novel object tracking algorithm based on compressed sensing and entropy of information," *Mathematical Problems in Engineering,* vol. 2015, 2015.

[6] C. Chen and J. Huang, "Compressive sensing MRI with wavelet tree sparsity," in *Advances in neural information processing systems*, 2012, pp. 1115-1123.

[7] Z. T. Harmany, R. F. Marcia, and R. M. Willett, "This is SPIRAL-TAP: Sparse Poisson intensity reconstruction algorithms—theory and practice," *Image Processing, IEEE Transactions on,* vol. 21, pp. 1084-1096, 2012.

[8] J. Bioucas-Dias and M. Figueiredo, "TwIST: Two-step iterative shrinkage/thresholding algorithm for linear inverse problems," ed: Feb, 2014.

[9] S. G. Mallat and Z. Zhang, "Matching pursuits with time-frequency dictionaries," *Signal Processing, IEEE Transactions on,* vol. 41, pp. 3397-3415, 1993.

[10] M. A. Figueiredo, R. D. Nowak, and S. J. Wright, "Gradient projection for sparse reconstruction: Application to compressed sensing and other inverse problems," *Selected Topics in Signal Processing, IEEE Journal of,* vol. 1, pp. 586-597, 2007.

[11] L. He and L. Carin, "Exploiting structure in wavelet-based Bayesian compressive sensing," *Signal Processing, IEEE Transactions on,* vol. 57, pp. 3488-3497, 2009.

[12] G. Rath and A. Sahoo, "A comparative study of some greedy pursuit algorithms for sparse approximation," in *Signal Processing Conference, 2009 17th European*, 2009, pp. 398-402.

[13] M. Fox, *Quantum Optics - An Introduction*.

[14] E. J. Candès, J. Romberg, and T. Tao, "Robust uncertainty principles: Exact signal reconstruction from highly incomplete frequency information," *Information Theory, IEEE Transactions on,* vol. 52, pp. 489-509, 2006.

[15] T. Tao. (2007). *Open Question: Deterministic UUP Matrices*.

[16] R. Baraniuk, M. Davenport, R. DeVore, and M. Wakin. (2008, 3). *A simple proof of the restricted isometry property for random matrices*.

[17] Y. C. E. a. G. Kutyniok, *Compressed Sensing Theory and Applications*. United States of America.

[18] A. A. Goldstein, "Convex programming in Hilbert space," *Bulletin of the American Mathematical Society,* vol. 70, pp. 709-710, 1964.

[19] E. S. Levitin and B. T. Polyak, "Constrained minimization methods," *USSR Computational mathematics and mathematical physics,* vol. 6, pp. 1-50, 1966.

[20] R. G. Baraniuk, V. Cevher, M. F. Duarte, and C. Hegde, "Model-based compressive sensing," *Information Theory, IEEE Transactions on,* vol. 56, pp. 1982-2001, 2010.

[21] H. Ishwaran and J. S. Rao, "Spike and slab variable selection: frequentist and Bayesian strategies," *Annals of Statistics,* pp. 730-773, 2005.

[22] M. F. Duarte, M. A. Davenport, D. Takhar, J. N. Laska, T. Sun, K. E. Kelly, *et al.*, "Single-pixel imaging via compressive sampling," *IEEE Signal Processing Magazine,* vol. 25, p. 83, 2008.

[23] M. A. Neifeld and J. Ke, "Optical architectures for compressive imaging," *Applied optics,* vol. 46, pp. 5293-5303, 2007.

[24] *Overview of Digital Micromirror Device*. Available: http://www.opticalsciences.com/dmd.html

[25] *Compressive Imaging: A New Single-Pixel Camera*. Available: http://dsp.rice.edu/cscamera

[26] T. Roelandts. (2014). *Gaussian noise is added, Poisson noise is applied*.

[27] D. F. W. a. G. J. Milburn, "Quantum Optics ".

[28] *Fock States* Available: https://en.wikipedia.org/wiki/Fock_state

[29] J. Fessler, *Chapter6 X-ray imaging: noise and SNR*, 2009.

[30] *Squeezed Light*. Available: http://www.squeezed-light.de/

[31] H. ARNOLDUS and T. GEORGE, "Conditions for sub-poissonian photon statistics in phase conjugated resonance fluorescence," *Optics communications*, vol. 87, pp. 127-133, 1992.